Annual Report April 1, 2012 - March 31, 2013

UTTAC-82, 2013

UTTAC

ANNUAL REPORT 2012

TANDEM ACCELERATOR COMPLEX
Research Facility Center for Science and Technology
University of Tsukuba

http://www.tac.tsukuba.ac.jp/

UTTAC

ANNUAL REPORT 2012

April 1, 2012 – March 31, 2013

UTTAC-82, 2013

Executive Editor: Eiji Kita
Editors: Hiromi Kimura, Daiichiro Sekiba, Kimikazu Sasa and Tetsuro Komatsubara

---

UTTAC is a series of issues, which include annual reports of
Tandem Accelerator Complex, Research Facility Center
for Science and Technology, University of Tsukuba.

Tandem Accelerator Complex, Research Facility Center for Science and Technology,
University of Tsukuba
Tennodai 1-1-1, Tsukuba, Ibaraki 305-8577, Japan

http://www.tac.tsukuba.ac.jp/
annual@tac.tsukuba.ac.jp

PREFACE

This annual report covers research conducted at the Tandem Accelerator Complex, Research Facility Center for Science and Technology, the University of Tsukuba, during fiscal year 2012 (April 1, 2012–March 31, 2013). After the 12UD Pelletron tandem accelerator was completely destroyed by the Great East Japan Earthquake on March 11, 2011, research has been limited to that using the 1 MV Tandetron accelerator and radiation source experiments, ^{57}Co Mössbauer spectroscopy, and positron annihilation spectroscopy. The circumstances of our research have not changed much and are almost the same as those in the last fiscal year. Thus, this volume has slightly fewer pages than older volumes.

We have started to reconstruct the main accelerator as a 6 MV tandem-type accelerator with support from the government through the Ministry of Education, Culture, Sports, Science and Technology (MEXT), Japan. We have completed the plan and design for the new 6 MV tandem accelerator, and it is being built by the National Electrostatics Corporation in Middleton, Wisconsin, USA. It is expected to arrive at Tsukuba at the end of February or the beginning of March 2014.

The efforts of Open Advanced Facilities Initiative supported by MEXT were continued in this term, and the second stage was completed. The extension to the next step has been decided, and, fortunately, the government will support additional facilities related to this program with an extra budget. With this support, our performance on this program will be accelerated and become more active in the next fiscal year.

We are looking forward to operating and reporting on the new 6 MV accelerator.

Editors

CONTENTS

6. LIST OF PUBLICATIONS

1.

ACCELERATOR AND EXPERIMENTAL FACILITIES

1.1 Accelerator operation 2012

K. Sasa, S. Ishii, H. Kimura, H. Oshima, Y. Tajima, T. Takahashi, Y. Yamato,
T. Komatsubara, D. Sekiba and E. Kita.

The University of Tsukuba Tandem Accelerator Complex (UTTAC) has operated and maintained the 1 MV Tandetron accelerator and the radio-isotope utilization equipment. In addition, the high resolution RBS/ERDA accelerator was installed at UTTAC in 2012. At present, we are developing the 6 MV Pelletron tandem accelerator instead of the broken 12UD Pelletron tandem accelerator which suffered serious damage from the Great East Japan Earthquake on 11 March 2011. The 6 MV Pelletron tandem accelerator will be installed and started formal operation in 2014.

The total service time of the UTTAC multi-tandem accelerator facility was 1,656 hours in the fiscal year 2012. 336 hours for the 1 MV Tandetron accelerator and 57 days for the radio-isotope utilization equipment were used for industrial users under the project "Promotion of Advanced R&D Facility Utilization", which was supported financially by the Ministry of Education, Culture, Sports, Science and Technology (MEXT) of JAPAN. In the project, a total of 16 research programs were conducted in 2012.

The 1 MV Tandetron accelerator

The operating time and the experimental beam time of the 1 MV Tandetron accelerator were 891.8 and 475 hours, respectively, during the total service time in 2012. A total of 55 research programs were carried out and a total of 509 researchers used the 1 MV Tandetron accelerator. Figure 1 shows the percentage of accelerated ions for the 1 MV Tandetron accelerator. ^{3}He was mainly used for a low-energy nuclear reaction for nuclear astrophysics. Figure 2 shows the percentage of research fields for the 1 MV Tandetron accelerator.

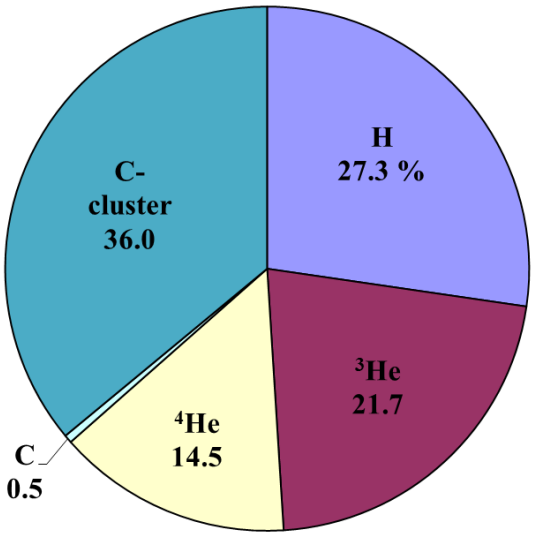

Figure 1. Percentage of accelerated ions for the 1 MV Tandetron accelerator in 2012.

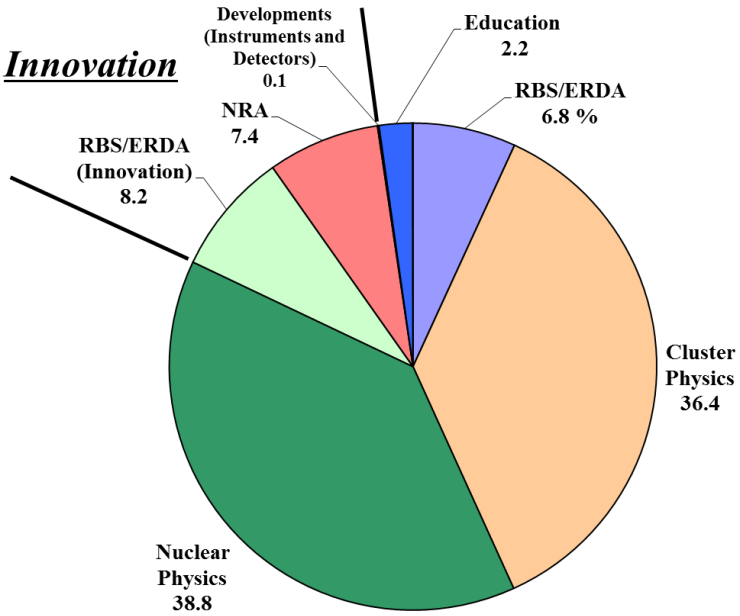

Figure 2. Percentage of research fields for the 1 MV Tandetron accelerator in 2012.

1.2 Status of the post-quake reconstruction project at UTTAC

K. Sasa, S. Ishii, H. Kimura, H. Oshima, Y. Tajima, T. Takahashi, Y. Yamato,
T. Komatsubara, D. Sekiba and E. Kita.

We are developing the post-quake reconstruction project to construct a new middle-sized tandem accelerator instead of the broken 12UD Pelletron tandem accelerator since it is difficult to repair the previous one due to some boundaries in the building construction. The accelerator system consists of a horizontal type 6 MV Pelletron tandem accelerator, new 4 ion sources and the Lam-shift polarized ion source (PIS), an accelerator mass spectrometry (AMS) system, ion beam analysis (IBA) systems and so on [1]. The PIS at the 9th floor of the building was damaged by the earthquake. After restoration of the PIS, it will be moved from the 9th floor to a new experimental booth at the ground. A high energy beam transport line will be connected from the accelerator room to the present experimental facilities at the experimental room. The magnets at the high energy side have a mass energy product of ME/Z^2 = 176 amu MeV. The beam transport line intersects with a new beam line for AMS and IBA at the accelerator room. The number of 12 beam lines will be available for nuclear physics and ion beam applications. In 2012, we completed the repair of the accelerator room. Figure 1 shows the photograph after the completion of renovation work on the accelerator room. Figure 2 shows the final layout of the 6 MV Pelletron tandem accelerator system.

Figure 1. Photograph of the accelerator room after the completion of renovation work.

The main accelerator, the model 18SDH-2 Pelletron tandem accelerator developed by National Electrostatic Corp. (NEC), USA, is a dual acceleration (tandem) electrostatic accelerator. The accelerator tank is designed as about 2.74 m in diameter and 8.77 m in length. The high voltage terminal has a longer gas stripper tube assembly and a foil changer with a 48 foil holders for equilibrium stripping ions. The stripper gas canal is about 10 mm in diameter and about 95 cm in length. The generator will operate reliably to terminal voltages as high as 6.3 MV. Figure 3 shows a layout of the main accelerator tank. Figure 4 shows a photograph of the main accelerator tank under development at NEC, USA. The accelerator will be capable of delivering up to 100 MeV for heavier ions. Maximum beam currents are estimated at about 3 μA for proton beam, and up to 50 μA for heavy ions. Table 1 shows specifications of the 6 MV Pelletron tandem accelerator.

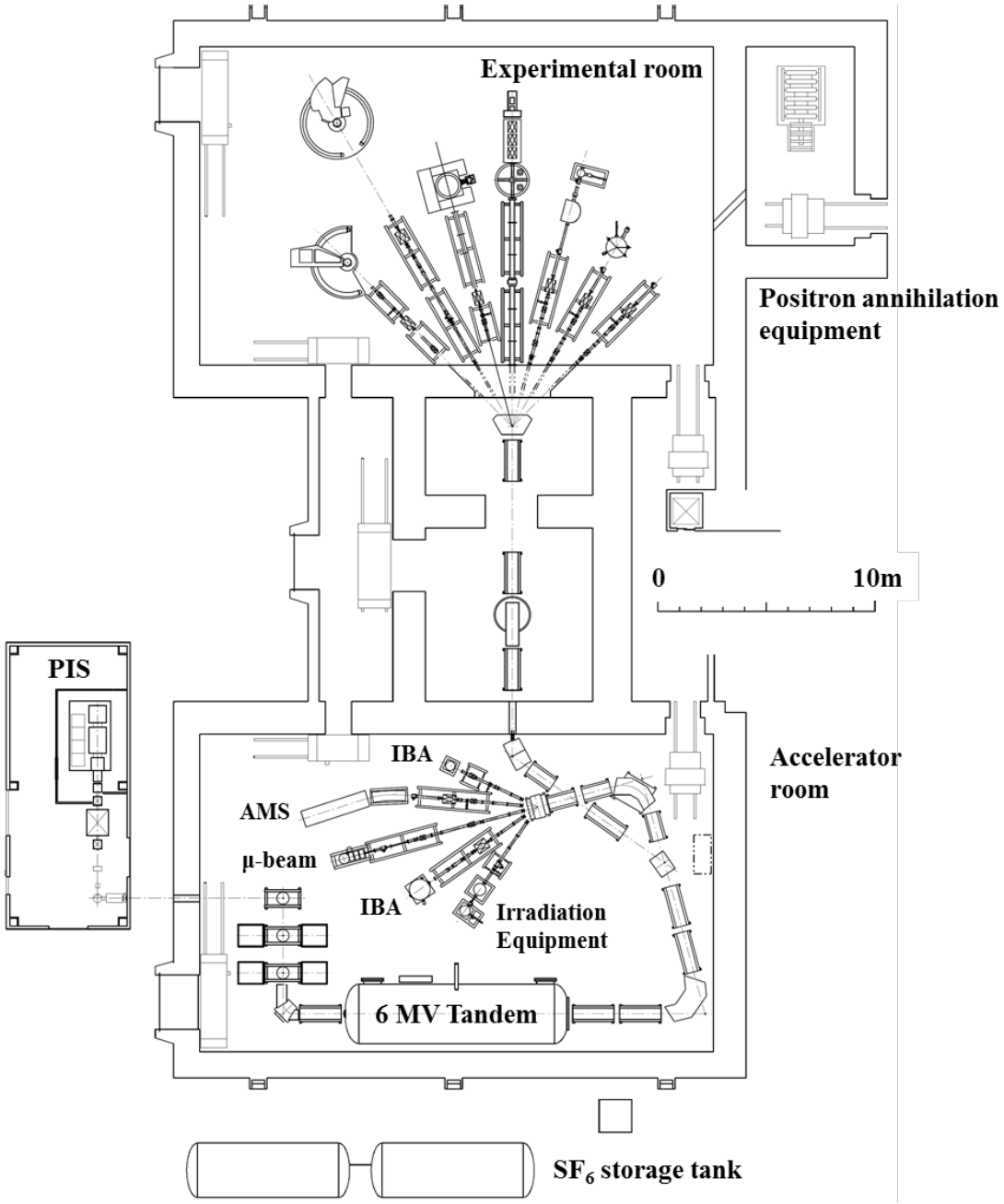

Figure 2. Final layout of the 6 MV Pelletron tandem accelerator system.

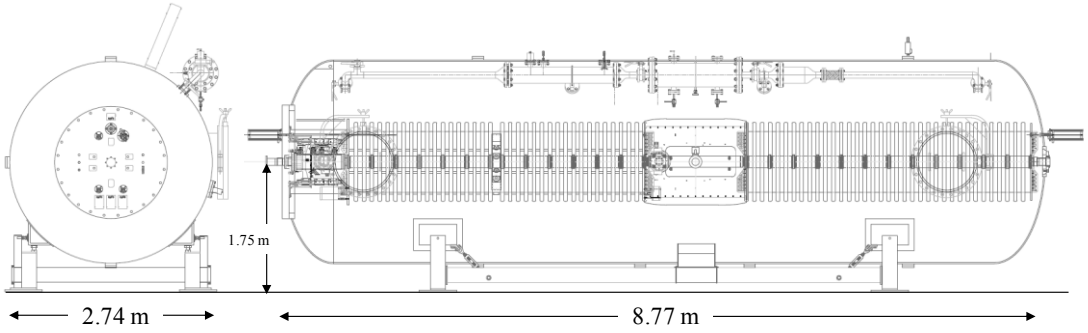

Figure 3. Layout of the model 18SDH-2 Pelletron accelerator tank.

Table 1. Specifications of the 6 MV Pelletron tandem accelerator.

Accelerator tank size:	
Length:	8.77 m
Diameter:	2.74 m
Beam line height:	1,775 mm
GVM and Slit current feedback system	
Terminal stripper:	
Gas (Ar or N_2)	
Foil unit (48 foil holders)	
Maximum Terminal Voltage:	6.5 MV
Maximum beam current:	
H:	3 μA
Heavy ions:	~50 μA (~Au)

Figure 4. Photograph of the accelerator tank at NEC, USA.

Figure 5 shows the low energy side and ion sources for the 6 MV Pelletron tandem accelerator. There are 3 rotational 90° electrostatic cylindrical analyzers (ESA) and 5 ion sources. We are also planning to install a CO_2 gas introduction system for one of the two MC-SNICS ion sources for ^{14}C-AMS.

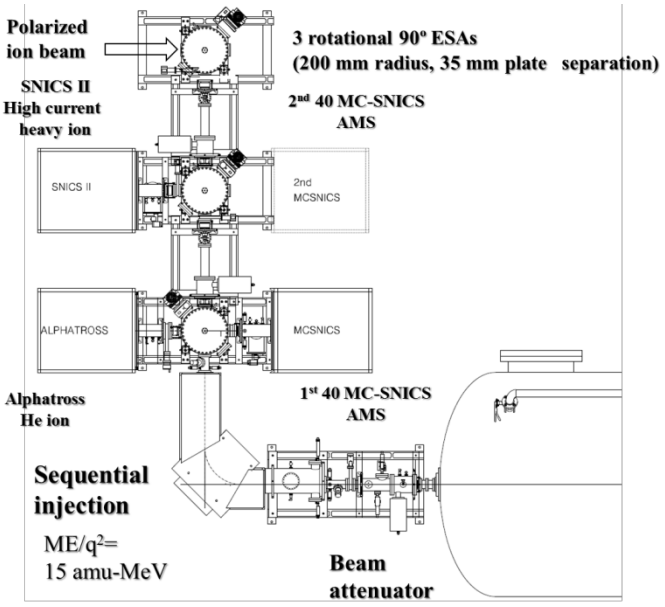

Figure 5. Low energy side and ion sources for the 6 MV Pelletron tandem accelerator.

In the field of nuclear physics, low-energy nuclear reaction, nuclear spin polarization and nuclear astrophysics are available in the new accelerator system. The 6 MV Pelletron tandem accelerator will be also applied to nanotechnology science, IBA, heavy ion irradiation and so forth. The rare particle detection system will be capable of measuring environmental levels of long-lived radioisotopes of ^{10}Be, ^{14}C, ^{26}Al, ^{36}Cl, ^{41}Ca and ^{129}I by AMS techniques. A 22.5° ESA with a 3.8 m radius is provided to filter out unwanted ions for AMS. The 22.5° ESA has a resolution of E/ΔE = 200. The rare particle detection system with a

five-electrode gas detector for AMS is provided to measure the rate of energy loss in the gas for each particle entering the gas detector chamber. The IBA system has a high-precision five-axis goniometer for RBS/ERDA and PIXE analysis. A micro-beam system will be equipped with Oxford OM2000 ion micro-beam end-stage with a triplet quadrupole lens assembly on the 0º beam course at the accelerator room. The micro-beam system is expected to focus ion beams less than 1 μm and apply to micro PIXE analysis and proton beam writing techniques. A charged particle irradiation equipment is mainly applied for radio resistance tests of space-use devices.

The construction of the 6 MV Pelletron tandem accelerator system is scheduled in the spring of 2014. The beam delivery will start on September 2014.

References

[1] Kimikazu Sasa et al., AIP Conf. Proc. 1533, pp. 184-188; doi: http://dx.doi.org/10.1063/1.4806798.

1.3 Measurement of the sign of the magnetic moment for proton by $\pi/2$ pulse NMR method with rotating magnetic field

D. Nagae, T. Niwa, Y. Abe, Y. Ishibashi, and A. Ozawa

A rotating magnetic field has been developing [1] to determine a sign of magnetic (μ) moment by the β-ray detected nuclear magnetic resonance (β-NMR) method [2]. A producing of the rotating magnetic field was achieved using an alternating current of about 5 MHz and two pairs of coils[3]. The measured polarization of the rotating magnetic field of approximately 90% was sufficient to applying the NMR. In order to investigate a perfomance of the rotating magnetic field, a measurement of the sign of the μ moment for proton ($\mu(\mathrm{proton}) = +2.792847351(28)\ \mu_N$) has been conducted by a $\pi/2$ pulse NMR method.

The measurement was performed by using an about 9-MHz alternating current and a proton sample (H_2O). The production method of the rotating magnetic field was essentially the same as that described in Ref.[1, 3]. A block diagram of the rotating magnetic field system and the $\pi/2$ pulse NMR system is shown in Fig. 1. The rotating magnetic field is obtained using two pairs of coils with axes crossed at right angles. The coil radius and distance of a pair of coil are 20 mm and 24 mm, respectively. The phase angles of the alternating currents for the two pairs of coils were shifted by 90°. Thus the resulting magnetic field was circularly polarized. By the adjustment of the phase-angle difference, a right- or left-circularly polarized magnetic field is produced. In order to obtained large polarized rotating magnetic field, amplitudes of each of the oscillating magnetic fields at resonance frequency were adjusted so as to make the outputs of a pickup coil equivalent. The crossed pair of coils and the proton sample were set at the center of a static magnet. In the $\pi/2$ pulse NMR method, a NMR is measured by detection of a Free Induction Decay (FID) which arises non-equilibrium nuclear spin magnetization precessing about the magnetic field. This non-equilibrium magnetization is induced by applying a pulse of resonant frequency of which direction is same as a Larmor precession of the nuclear spins. A static magnetic field of approximately 2.1 kG was applied to preserve a spin polarization with a direction from bottom to up. In this case, the FID signal is

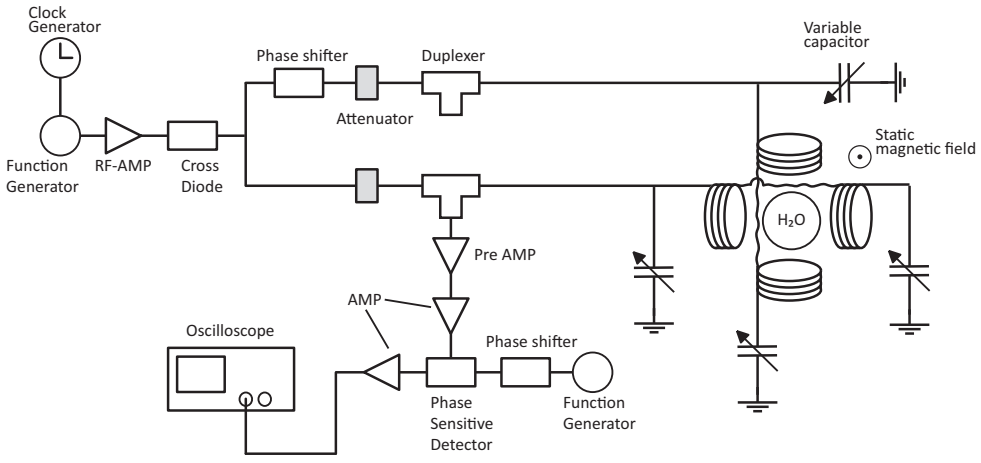

Fig. 1. A block diagram of the $\pi/2$ pulse NMR with rotating magnetic field.

obtained when a right-circularly polarized magnetic field is applied. The FID signal of which frequency is same as a resonant frequency was detected by the pairs of coil, then the signal sent to a oscilloscope through amplifiers and a phase sensitive detector (PSD). A reference signal of which frequency was set as 9.00 MHz was provided by an another function generator and then was sent to the PSD via a phase shifter. A phase of the reference frequency was adjusted so as to the FID signal was maximum. The measurements were carried out in the following sequence. The rotating magnetic field perpendicular to the static field was applied to the proton for a 55 μs duration using the pairs of coils. The FID was measured during the following 1 s.

The FID signals obtained by applying left- and right-circularly polarized magnetic field are shown in Fig. 2 a and b, respectively. The yellow and green signals indicate a FID signal and a start signal of rotating magnetic field. In the FID signals, a noise might be due to the rotating magnetic field was observed. Nevertheless, a larger FID signal is clearly observed when the right-circularly polarized magnetic field was applied as shown in Fig. 2 b. Taking account of the direction of the spin polarization (bottom to up), it is successfully confirmed that the sign of the μ moment for proton is positive.

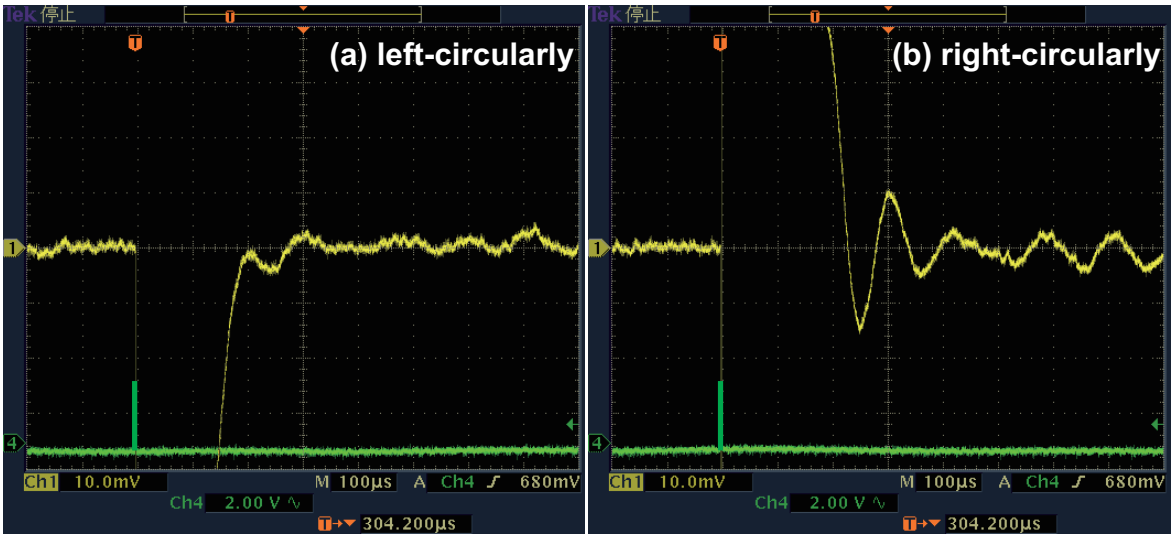

Fig. 2. FID signals obtained by applying left- and right-circularly polarized magnetic field.

References

[1] T. Niwa et al., UTTAC annual report 2011, UTTAC-81, 5(2012).

[2] K. Sugimoto et al., J. Phys. Soc. Jpn., **21**, 213(1966)

[3] D. Nagae et al., Hype. Int., **220**, 65(2013).

[4] G.S. Bales et al., Phys. Rev., **B50**, 6057(1994).

2.

NUCLEAR PHYSICS

2.1 Investigation of Big Bang nucleosynthesis for solving ^{7}Li problem

T. Komatsubara, T. Yuasa, T. Onish, K. Sasa, A. Ozawa, S. Okada, Y. Saito, T. Shizuma[1], T. Hayakawa[2], S. Kubono[2]

One of the most important success for the theory of nucleosynthesis is the precise reproduction of the mass abundance ration for helium-4 as 25% in the Big Bang nucleosynthesis (BBN) [1]. This achievement can be one of the three proves of the existence of the Big Bang. Others are the red shift and the cosmic microwave background. For the comparisons between the theoretical calculations and the observations, abundances of deuteron and helium-3 are also consistent. However, for litium-7 there is a large discrepancy which the theory is three times higher than the observations [2] in spite of the resent theoretical efforts [3]. Here, the observed abundance is referred from the plateau values in metal poor stars reported by Spite [4] and/or Asplund [5]. In order to solve this large inconsistency, studies of the nuclear reaction cross sections around the ^{7}Li have been started. In the case of ^{7}Li(^{3}He, p_0)^{9}Be reaction the experimental information is not sufficient between 0.1 and 0.4 MeV of the c.m. energy [6,7]. In this report, our progress of the cross section measurements will be presented and shown as the astrophysical S-factor.

The measurements of the reaction cross sections have been performed at UTTAC by using 1MV tandetron. An enriched ^{7}Li target was irradiated by ^{3}He beam. The enrichment of the ^{7}Li is 99%. The target was made by evaporation method of the metal on a carbon substrate of 50 mg/cm^2 thickness. The thickness of the ^{7}Li target is estimated to be 18.1±1.3 μg/cm^2 for 0.5 MeV measurement and 24.8±1.8 μg/cm^2 for others by comparison with the previous report done by Sanada [8].

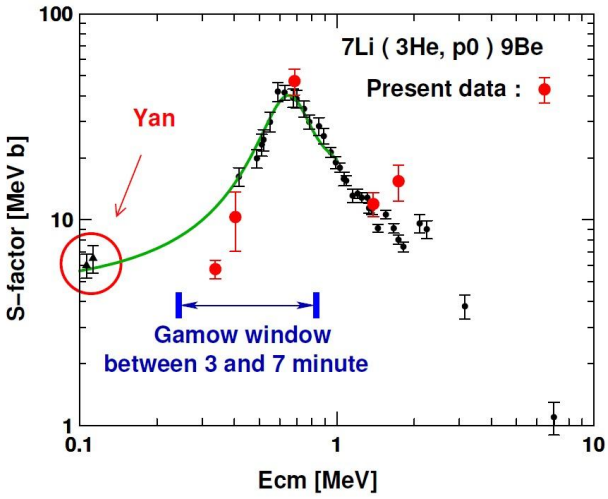

Fig. 1 Astrophysical S-factors for the ^{7}Li(^{3}He, p_0)^{9}Be reaction. Present results are shown as red circles. The Gamow window for BBN between 3 and 7 minutes is shown by the arrow. The green solid line shows the previous interpolation done by Yan [6].

As the results of the experiments the astrophysical S-factors are shown in figure 1. The present results are shown as red circles which correspond to E_{lab} = 0.5, 0.6, 1.0, 2.0, 2.5 MeV bombarding energies. The abscissa is the calculated effective c.m. energies. Black triangles appearing around 0.1 MeV are the reported values by Yan [6], and the black circles above 0.4 MeV are by Rath [7]. The green solid line shows the previous interpolation by Yan [6]. The Gamow

[1] Japan Atomic Energy Agency, Tokai, Ibaraki 319-1106, Japan
[2] RIKEN, Wako, Saitama 351-0198, Japan

window which corresponds to the range between 3 and 7 minutes at BB is shown by the arrow. The present result at $E_{c.m.}$=0.34 MeV is obviously lower than the previous interpolation. Then this results might lead smaller destruction of ^{7}Li.

Acknowledgment

We would like to express my gratitude for their helpful support by all staff and secretaries at the University of Tsukuba, Tandem Accelerator Complex. This work has been supported in part by Grants-in-Aid for Scientific Research (21340068, 21540295, 24540298) of Japan.

References

[1] R.V. Wagoner, Astrophysical Journal 148, 3 (1967) and D.N. Schramm, Review of Modern Physics, 70, 303 (1998).
[2] A. Coc, Physical Review D 65, 043510 (2002).
[3] M. Kusakabe, The Astrophysical Journal, 680, 846-857, (2008).
[4] F. Spite, Astronomy and Astrophysics, 115, 357 (1982).
[5] M. Asplund, The Astrophysical Journal, 644, 229-259, (2006).
[6] J. Yan, Physical Review C 65, 048801 (2002).
[7] D.P. Rath, Nuclear Physics A 515, 338 (1990).
[8] J. Sanada, J. Phys. Soc. Japan 26, 853 (1969).

2.2 In-beam γ-ray spectroscopy of ^{30}P via the ^{28}Si(^{3}He, $p\gamma$)^{30}P reaction

E. Mcneice[1], K. Setoodehnia[1], B. Singh[1], Y. Abe, D. N. Binh[2], A. A. Chen[1], J. Chen[1], S. Cherubini[3], S. Fukuoka, T. Hashimoto[2], T. Hayakawa[4], Y. Ishibashi, Y. Ito, D. Kahl[2], T. Komatsubara, S. Kubono[2], T. Moriguchi, D. Nagae, R. Nishikiori, T. Niwa, A. Ozawa, T. Shizuma[4], H. Suzuki, H. Yamaguchi[2], T. Yuasa

^{30}P is an odd-odd self-conjugate nuclide, whose level density is reasonably high (34 proton-bound excited states below $S_p = 5594.5(3)$ keV [1]) relative to that in the neighbor isobars. Isospin $T = 0$ and $T = 1$ excited states coexist in ^{30}P from the ground state upwards. Such isospin symmetry breaking can change the statistical distribution of electromagnetic transitions [2] and have a large impact on the level statistics [3]. Spectroscopy of ^{30}P thus provides an experimental test of the effect of isospin symmetry breaking.

Despite several previous measurements [4], the γ-ray transitions of several states in ^{30}P have never been observed before, and many of the proton resonances with $E_x > 5.7$ MeV still have tentative spin-parity assignments.

The ^{28}Si(^{3}He, $p\gamma$)^{30}P reaction was the main background channel in an in-beam γ-ray spectroscopy experiment previously performed [5, 6] to investigate the level structure of ^{30}S populated via the ^{28}Si(^{3}He, $n\gamma$)^{30}S reaction. Thus, we analyzed the existing data corresponding to the former channel to investigate whether or not we could improve our understanding of the level properties of ^{30}P. We specifically aimed to explore the region just above the proton threshold, where the γ-rays from decays of a number of resonances whose excitation energies are near 6 MeV have never been observed before [4].

To carry out the original experiment, a ^{3}He^{2+} beam was accelerated via the tandem accelerator at the UTTAC to 9 MeV and was impinged on a self-standing 25 μm-thick foil of natural silicon. The experiment consisted of two phases, which are explained in full details in Refs. [7, 8]. Our γ-ray detector setup consisted of two high-purity Ge-detectors located at 90° (phase I), and 90° and 135° (phase II) with respect to the beam axis and on the opposite sides of the beam line. In each phase of the experiment, a γ-γ coincidence matrix was produced and analyzed to obtain information on ^{30}P decay scheme.

In our γ-ray angular distribution measurement, the intensities of the strong ^{30}P γ-ray transitions observed in the singles spectra were normalized to the intense 677.1-keV $0^+ \rightarrow 1^+$ transition in ^{30}P. The normalized relative yields for each peak of interest were plotted against the detection angle, and these data were fitted using the Legendre polynomials. The γ-γ angular correlations of ^{30}P γ-rays were determined by measuring the directional correlations of oriented states for the strong ^{30}P γ-ray transitions.

After placing software coincidence gates on the strong ^{30}P peaks observed in the singles spectra, decay cascades from higher-lying states were observed in the γ-γ coincidence spectra (see Fig. 1). By performing a least-squares fit to the recoil corrected γ-ray energies, the ^{30}P excitation energies were reconstructed to obtain the level scheme of ^{30}P. For the sake of brevity, we have not shown the tabular results here. They will be available online at the Experimental Unevaluated Nuclear Data List (XUNDL) database [10]. A

[1]Department of Physics & Astronomy, McMaster University, Hamilton, ON L8S 4M1, Canada
[2]Center for Nuclear Study, University of Tokyo, Wako Branch at RIKEN, 2-1 Hirosawa, Wako, Saitama, 351-0198, Japan
[3]Dipartimento di Fisica e Astronomia, Università di Catania, Catania, Italy
[4]Japan Atomic Energy Agency, Japan

summary of our results will be published in Ref. [11].

We have observed for the first time 47 new transitions from ^{30}P excited states, most of which are proton resonances. Observation of these new transitions has enabled us to reduce the uncertainties (from 3 – 10 keV down to $<$ 1 keV) on the excitation energies of 17 states, denoted by † in Table 1 of Ref. [10], for which no γ-ray transitions have been observed prior to the present work. Figure 1 presents a sample of the coincidence spectrum obtained during phase I from a coincidence gate on a newly observed 1946.5-keV peak, revealing several additional transitions from the ^{30}P excited states.

With the results of our γ-ray angular distribution and γ-γ directional correlation measurements, we have been able to confirm the previously determined spins of several states in ^{30}P. However, over all, our data are not adequate to assign firm spins to the other observed levels whose spin-parity assignments were previously determined to be tentative.

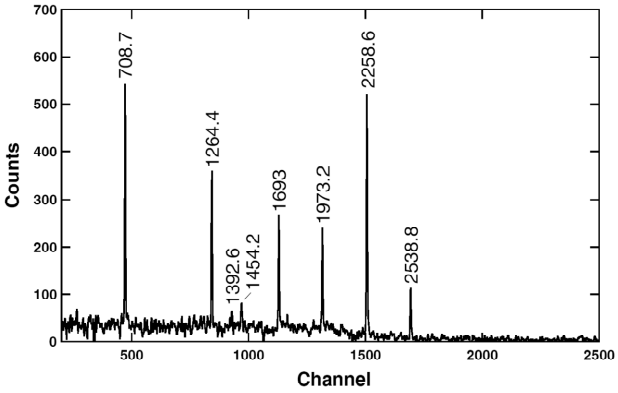

Figure 1: A sample of γ-γ coincidence spectrum measured at 90° obtained from gating on the 1946.5-keV (with $J^\pi = (6)^+ \rightarrow J^\pi = 4^-$) transition of ^{30}P, which is observed here for the first time. Peaks are labeled with their energies (in keV) that are weighted averages between both phases of the experiment. The 1946.5-keV γ-ray de-excites the 6178.50(17)-keV excited state of ^{30}P. Based on the results of Refs. [9, 12], and those of the present work, we have assigned $J^\pi = (6)^+$ to this state. A recent shell model calculation [13] predicts a $J^\pi = 5^+$ state within 100 – 200 keV from the 6178.50(17)-keV state observed in the present work. Our data do not rule out $J^\pi = 5^+$ (with the $E1$, $M2$ mixing ratio of $\delta \approx 0.5$) for the 6178.5-keV state.

References

[1] G. Audi, M. Wang, A. H. Wapstra *et al.*, Chinese Phys. C 36 1287 (2012).

[2] J. F. Shriner Jr., C. A. Grossmann, and G. E. Mitchell, Phys. Rev. C 62 054305 (2000).

[3] J. F. Shriner Jr., E. G. Bilpuch, and P. M. Endt, Z. Phys. A 335 393 (1990).

[4] M. S. Basunia, Nucl. Data Sheets 111 2331 (2010).

[5] K. Setoodehnia, A. A. Chen, T. Komatsubara *et al.*, UTTAC Annual Report 2009, UTTAC-79 p. 9 (2010).

[6] K. Setoodehnia, A. A. Chen, T. Komatsubara *et al.*, UTTAC Annual Report 2010, UTTAC-80 p. 9 (2011).

[7] K. Setoodehnia, A. A. Chen, T. Komatsubara *et al.*, Phys. Rev. C 83 018803 (2011).

[8] K. Setoodehnia, A. A. Chen, D. Kahl *et al.*, Phys. Rev. C (submitted), arXiv:1210.1194 (2012).

[9] C. A. Grossmann, M. A. LaBonte, G. E. Mitchell *et al.*, Phys. Rev. C 62 024323 (2000).

[10] Experimental Unevaluated Nuclear Data List: *http://www.nndc.bnl.gov/ensdf/ensdf/xundl.jsp*.

[11] E. Mcneice, K. Setoodehnia, B. Singh *et al.*, Proceedings of International Conference on Nuclear Data for Science and Technology, New York, March (2013).

[12] B. Ramstein, L. H. Rosier, and R. J. De Meijer, Nucl. Phys. A 363 110 (1981).

[13] Alex Browne, (private communication).

2.3 Investigation of nuclear reactions for silicon burning around scandium-45

T. Onishi, T. Komatsubara, A. Ozawa, K. Sasa, D. Izumi, M. Mukai, S .Kubono[1],
T. Hayakawa[2], T. Shizuma[2]

Elements up to iron are created by the burning process in star. There are various processes, but we took an interest in silicon burning which is the final stage of nucleosynthesis in star. The silicon burning starts from photodisintegration by high-energy gamma-ray and alpha-capture of silicon. Then, various elements are created through quasi-equilibrium process. The reaction flow of quasi-equilibrium process is complex and there are many reactions around scandium-45 [1]. The aim of our study is to measure reactions around scandium-45 which is known as a bottleneck in silicon burning. Woosly[1] pointed out that the flow is concentrated to ^{42}Ca(α,p)^{45}Sc and ^{45}Sc(p,γ)^{46}Ti reaction. In order to evaluate nuclear reaction rate of the ^{42}Ca(α,p)^{45}Sc, we have performed measurements of the cross section and angular distribution for the inverse reaction of ^{45}Sc(p,α)^{42}Ca(Q-value = 2.34MeV). For this reaction, the experimental data were limited only above 2.8MeV [2]. Therefore, we measured ^{45}Sc(p,α)^{42}Ca reaction between 1.8MeV and 2.1MeV. This energy range corresponds to Gamow peak at a temperature of about 3GK in silicon burning. Also, we examine minutely the region between 2MeV and 2.1MeV in order to confirm whether the resonance structure exists.

Our measurements were carried out by 1MV Tandetron accelerator at UTTAC. The accelerated proton beam was irradiated on scandium target. The scandium target was prepared by evaporation in vacuum on to 50 μg/cm^2 crabon backing. The thickness of scandium layer was measured to be 42 μg/cm^2. Alpha-particle from ^{45}Sc(p,α)^{42}Ca reaction was measured with E-Δ E counter by using SSD. We measured detector angle with magnescale to evaluate angular distribution.

As a result, alpha-particle from ^{45}Sc(p,α)^{42}Ca reaction was separately measured from strong elastic scattering of protons by ^{45}Sc layer and carbon backing. The yields of alpha-particle are corrected by dead time of DAQ. The relation of the yield and the cross section is represented by following equation,

$$Y = n\frac{N}{S}\frac{d\sigma}{d\Omega}\Omega$$

where Y is yield, n is number of incident proton, N/S is particle area density of scandium45, dσ/dΩ is differential cross section and Ω is solid angle. The differential cross section is calculated by using this equation.

Figure 1 shows angular distribution for differential cross section of ^{45}Sc (p,α)^{42}Ca reaction for 2MeV. Differential cross section of forward angle seems to increase by contribution of direct component. We think that of backward angle is compound component. We have compared the differential cross section

[1]RIKEN,Wako, Saitama 351-0198, Japan
[2]Japan Atomic Energy Agency, Tokai, Ibaraki 319-1106, Japan

data at 130° for each energy and found the possibility of the existence of resonance structure. However, we have not finished analyzing.

In future, we will calculate total cross section from angular distribution and evaluate astrophysical S-factor. Furthermore, we will perform detailed analysis of resonance structure.

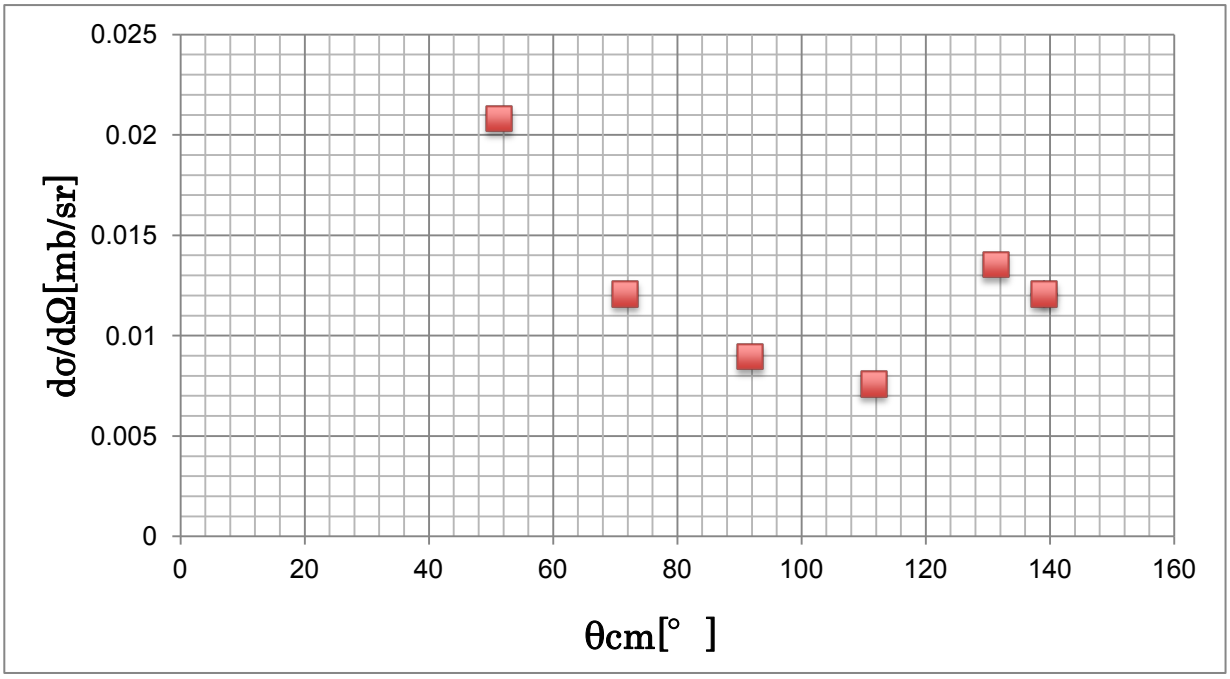

Fig.1 Angular distribution of differential cross section for $^{45}Sc(p,\alpha)^{42}Ca$ in CMS

References

[1]S.E. Woosly, W. David Arnett, Donald D. Clayton, Astrophys J.S.231,26(1973) 231-312.

[2]J.S. Schweitzer, Z.E. Switkowaki, R.M. Wieland, NPA 287 (1977) 344.

2.4 Measurements of nuclear moments for unstable nuclei in AVF, RCNP

T.Niwa, Y.Abe, Y.Ishibashi, D.Nagae, S.Okada, A.Ozawa, K.Hatanaka[1]

By the Great East Japan Earthquake on Mar. 11, 2011, 12UD accelerator in UTTAC has been completely destroyed and the experimental programs related to measurements of nuclear moments for unstable nuclei in UTTAC [1] has been stopped. In this situation, research center of nuclear physics (RCNP), Osaka University, offered to provide the machine-time which was terminated by the earthquake. We accepted this support and started to build our experimental apparatus for β-NMR system, which can be used for measurements of nuclear moments for unstable nuclei, in AVF facility, RCNP from 2012. In this report, we will introduce the apparatus built in AVF, RCNP, and show preliminary results for the performance test using the apparatus.

Experimental apparatus, which we built in AVF, RCNP, is shown in Fig. 1. A NMR magnet, which was newly constructed by using the reconstruction budget through the Ministry of education, Culture, Sports, Science and Technology Japan, was transported from Tsukuba to RCNP. The connection part from AVF cyclotron to a NMR chamber located in the center of the NMR magnet was built by RCNP. The NMR chamber and the detectors to measure the β-rays are reused in those used in UTTAC [1].

The performance check of the apparatus was done in July, 2012. We performed a measurement of the magnetic moment of ^{24m}Al (I=1$^+$, $T_{1/2}$=131.3 ms) by using this apparatus. The magnetic moment of ^{24m}Al has been measured in HIMAC, NIRS [2]. The nuclear polarized ^{24m}Al has been produced by the ^{24}Mg($\vec{p}$, n)^{24m}Al reaction with a polarized proton beam. The proton polarization was optimized by using a simple polarimator made of two plastic scintillators located at the down stream of the NMR chamber (see Fig. 1). The primary proton beam energy was 53 MeV and the intensity was 16 nA. A target, which can also become a stopper for the recoiled ^{24m}Al, was a MgO crystal (0.5 mm thickness). β-rays emitted from the polarized ^{24m}Al were measured by two sets of beta-ray telescopes located above and below of the stopper. Each set of the telescope consists of two thin plastic-scintillators (1 mm thickness), a Cu absorber (1 mm thickness) and a thick plastic-scintillator (10 mm thickness). Observed time-spectrum of the β-rays confirmed the ^{24m}Al production in the target. Preliminary observed β-NMR spectrum is shown in Fig. 2, where the magnetic field of the NMR magnet was set to be 2.413 kG. This magnetic field corresponds to 5.5 MHz Larmor-frequency for ^{24m}Al. We observed about -0.4% effective asymmetry for ^{24m}Al.

As the summary, we built the β-NMR apparatus in AVF facility in RCNP, which is a part of the support program for the Great East Japan Earthquake in RCNP. The preliminary measurement for the magnetic moment of ^{24m}Al shows that the present apparatus can be used for the measurements of nuclear moments for some unstable nuclei by the β-NMR method. Thus, by using the apparatus, we will continue the experimental programs performed in UTTAC.

[1] RCNP, Osaka University

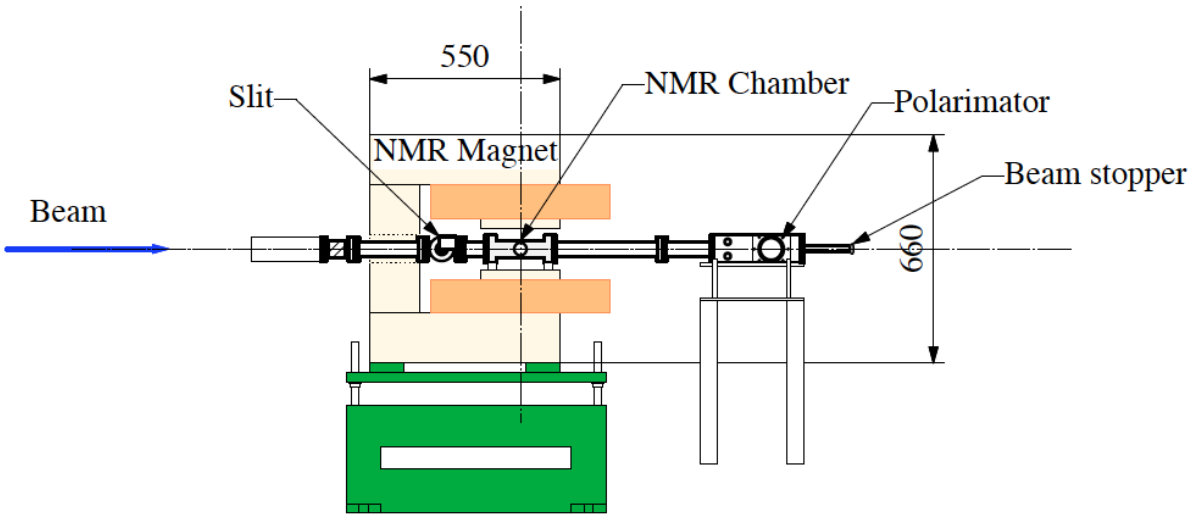

Fig.1 A side view of experimental apparatus built in AVF, RCNP. A MgO target (stopper) is located in the middle of the NMR chamber.

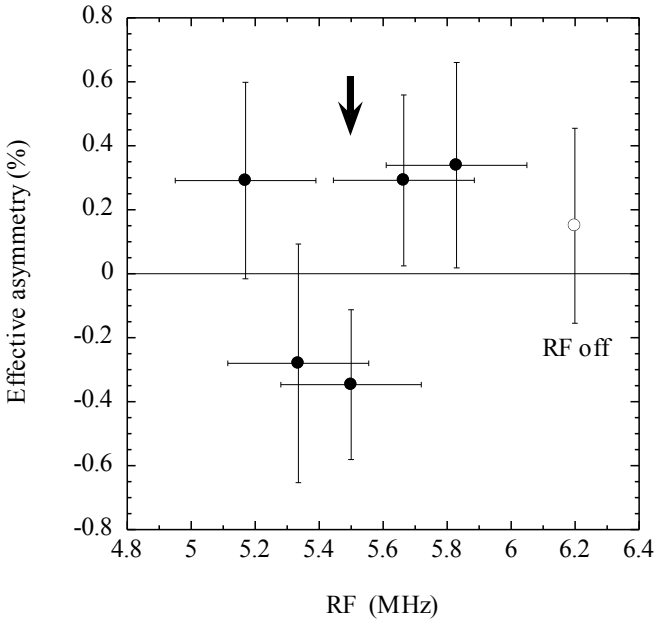

Fig. 2 Frequency dependence of the effective asymmetry for ^{24m}Al observed in our apparatus. Open circle corresponds to the data without RF. Arrow corresponds to Larmor frequency of ^{24m}Al with 2.413 kG magnetic field.

References

[1] Y.Ishibashi et al., UTTAC ANNUAL REPORT 2010 (2011) 17. and References therein.

[2] D.Nishimura et al., Hyperfine Int. 180 (2007) 71.

2.5 Time resolution measurements for the time-of-flight detector in HIMAC

S. Okada, D. Nagae, A. Ozawa, Y. Ishibashi, Y. Abe, S. Fukuoka, R. Nishikiori, T. Niwa, Y. Saito, N. Inaba, S. Aldyyarov, K. Sawahata

The precision mass measurement system of rare RI beam is proposed at RIKEN RI beam factory (RIBF) [1]. In this plan, the masses are deduced from a time-of-flight (TOF) of RIs in the ring. Details of a principle of a mass measurement are described elsewhere [2]. In order to determine masses with a precision of 10^{-6}, a time resolution less than 100 ps is needed. A dedicated TOF detector using a micro channel plate (MCP) and a carbon foil has been developed (MCP-TOF) [3]. A schematic view of the MCP-TOF is shown in Fig. 1. A principle of the MCP-TOF is explained in Ref. [3]. The size and thickness of the carbon foil is 100 mm × 50 mm and 60 μg/cm^2. Nine electrodes which are connected 2.2 MΩ resisters at 5.0 mm intervals are installed in the MCP-TOF to create a uniformed electric field. To make a magnetic field, two coils are placed both side of the MCP-TOF. To achieve of isochronous condition for electron is emitted from the carbon foil, the relation between the electric (E), and the magnetic (B) fields and a lateral displacement of the secondary electrons (D) is given by [4]

$$D = \frac{2\pi m}{q}\frac{E}{B^2}$$

where m and q denotes a mass and a charge of electron, respectively. In the case of the present MCP-TOF, the lateral displacement and the electric field are set at D = 140 mm and E = 60 V/mm, thus the magnetic field is calculated to be B = 39.1 G. To obtain good time resolution, it is important that good homogeneous magnetic and electric fields.

In this work two modifications were made to obtain homogeneous magnetic and electric fields. Concerning of the magnetic field, the number of right coils was adjusted from 100 turns to 94 turns. In this adjustment, an inhomogeneity of the magnetic field was reduced from 15% to 7%. For the electric field, a ground electrode which is opened on one side was replaced to a full opened one with grids made of Au + W wire with a diameter of 12 μm as shown in Fig. 2. As the result of the modification, a uniform distribution of the electric field was improved around ground electrode.

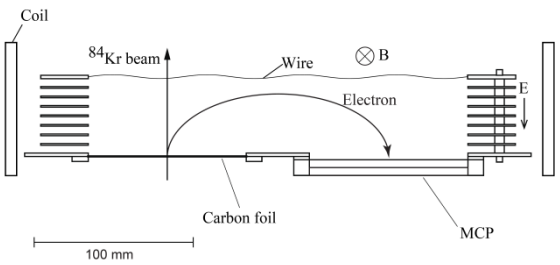

Fig. 1 Schematic view of the MCP-TOF

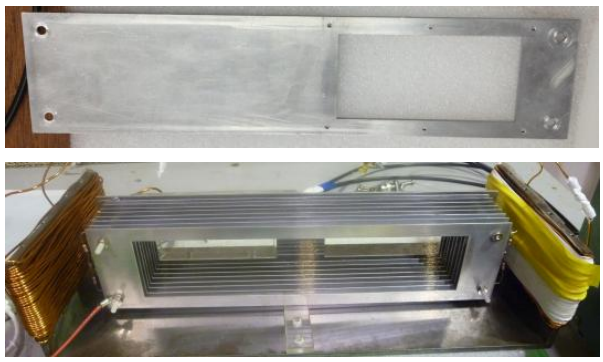

Fig. 2 (a) Previous ground electrode (b) Replaced ground electrode and MCP-TOF

An experiment to evaluate a time resolution of the MCP-TOF was conducted at SB2 beam line in HIMAC. The experimental set up is shown in Fig. 3. ^{84}Kr beam (200 *A* MeV) was transported to the MCP-TOF. In order to obtain the time resolution, a TOF between a trigger detector and the MCP-TOF was measured. As the trigger detector, a 1-mm-thick plastic scintillator of which both ends were connected on photomultiplier tubes was used. Two parallel plate avalanche counters (PPAC) were used to measure the position distribution of the beam and to obtain the beam profile at the carbon foil by a ray-trace technique. To measure total energy of the beam, an NaI(Tl) detector was set the downstream of the detectors. A typical TOF spectrum is shown in Fig. 4. In this measurement, the magnetic field was adjusted to 41.5 G so as to the TOF spectrum was narrow. The time resolution is obtained by fitting the TOF spectrum with a Gaussian function. The obtained width of the peak includes the intrinsic resolution of the trigger detector, which is σ= 50 ps. By subtracting the contribution of the trigger detector, preliminary intrinsic time resolution was deduced as $\sigma \approx$ 175 ps.

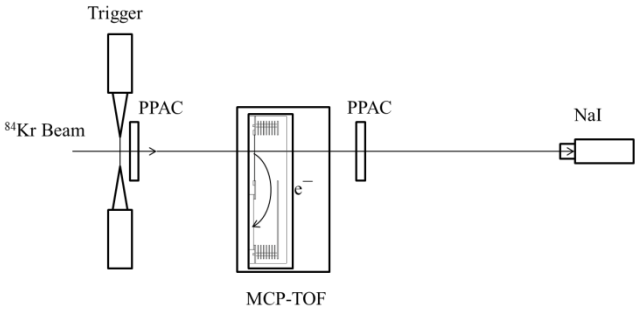

Fig. 3 Experimental setup

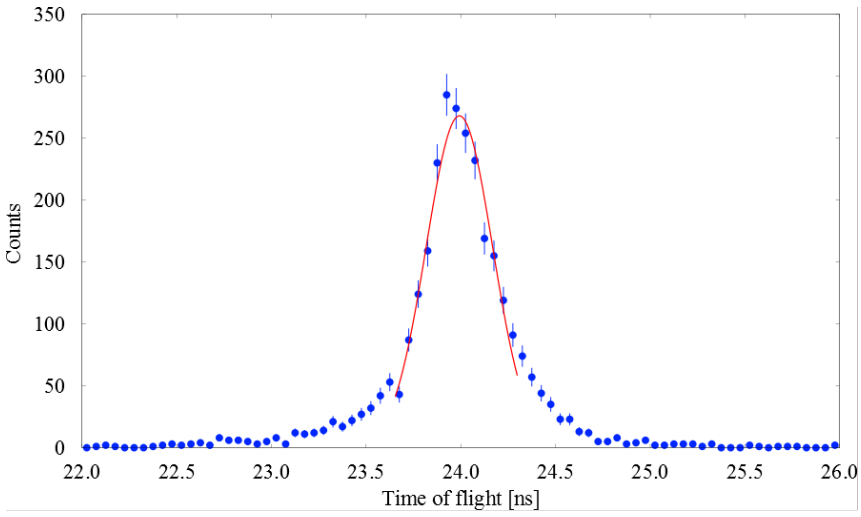

Fig. 4 TOF spectrum. The red solid line is a fit of data points by a Gaussian.

References

[1] Y. Yano, Nucl. Instr. and Meth. B 261 (2007) 1009.

[2] Y. Yamaguchi, *et al*., Nucl. Instr. and Meth. B 266 (2008) 4575.

[3] Y. Abe, *et al*., UTTAC Annual Report 2010, UTTAC-80 p. 19 (2011).

[4] J. D. Bowman, R. H. Heffner, Nucl. Instr. and Meth. 148 (1978) 503.

3.

MATERIALS AND CLUSTER SCIENCE

3.1 Zero Degree Electron Spectroscopy of 16 MeV C_2^+ Ions

S. Tomita, S. Funada, Y. Shiina, K. Sasa, M. Sataka[1], M. Matsuda[1], M. Imai[2], K. Kawatsura[3]

The yields of secondary electron Y_e induced by swift ions are well known to be almost proportional to the electronic stopping power S_e of incident charged partilcles, $Y_e = \Lambda S_e$, where Λ is called material parameter. The relation holds wide range of materials over the four order of incident energy, not only for protons but also for heavy atomic ions[1], except of some special cases. Strong suppression of secondary electron yeild for molecular ion beam is one of example of the special case. The supression effect of secondary electron per number of incident atom for 0.5 MeV/atom C_4^+ is almost 50% of that of atomic ion with same velocity[2]. Since the electronic stopping power of C_4^+ is almost same as that of atomic ion[3], the supression mechanism should take place in the process of either transport of scattered electrons inside material or transmission of scattered electrons through material surface.

Recently, we have reported that the convoy electron yield per number of incident atom is almost linear to the number of incident atom. These electrons can be considered to be mainly generated by the capture of scattered electron to the continuum state of the projectile on the emergence from target surface. Therefore, the result implies that the amount of scattered electron inside the target material with same velocity as projectile atom should be almost linear to number of incident atoms. To shed a light on these phenomena related to the transport of scattered electron inside target material, we have performed zero degree electron spectroscopy with swift molecular ions.

The experiments were performed with ion beams provided by the tandem accelerator of the Japan Atomic Energy Agency, Tokai. C_2^+ ions were produced by ECR ion source from benzen gas. The ion source was located on the high voltage terminal of the tandem accelerator. The ions were extracted by potential difference of 10 kV and injected to the normal acceleration beam line by a 90° magnet. The mass selected ions using a 180° magnet on the high voltage terminal, the ions were injected to the acceleration tubes. The accelerated ions were mass selected again by 90° bending magnet and transported to the experimental chamber.

The experimental apparatus used for the present experiment is described elsewhere in detail[4]. The ions were injected on the target of thin carbon foil purchased from Arizona Carbon Foil Co. Inc.. The nominal thickness was 3μg/cm^2. On the down stream of the target, 45° tandem parallel-plate spectrometer was placed at zero degrees with respect to the direction of projectile ion beam. The resolution of the spectrometer is 3.2% without the deceleration of the electrons before entrance of second analyzer.

The obtained energy spectrum for 16 MeV C_2^+ is shown in Fig.1. The prominent paek at 366 eV corresponds to the convoy electrons which have same velocity as projectile ions. The other peak at 1.2 keV is the KLL Auger electrons from projectile ions. The energy corresponds that of C^{3+} ion reported to be 230 eV in projectile frame[5]. In addition to the two peaks, thre is also two peaks of Coster-Kronig transition, which can be found as a shoulder on the both energy side of the convoy peak. It is not possible to determine the exact transition channel of the peak, due to poor energy resolution. But the position of

[1]Japan Atomic Energy Agency
[2]Kyoto University
[3]Kansai Gaidai University

peaks agree roughly with the value reported by Yamazaki[6] for C^{3+}+He collisions.

The electron yields of convoy electron, Coster-Kronig transition, and binary election for C_2^+ are compared with that for C^+ ion with same velocity and tabulated in Table1. Here we use the yield of KLL Auger electrons for the normalization, because the strong cluster effect is not expected for does not the inner shell electron excitation process. The cluster effect for the convoy electron yield is 4.3 which does not agree with the linearity reported for 0.5 MeV/atom C_n^+ ions. We think that this value stems from both cluster effect and loss electron, because of rather thin carbon foil thickness. The yield of Coster-Kronig transition also shows cluster effect, which could stems also from thin target thickness, which will results higher yield of low charge state for molecular beam.

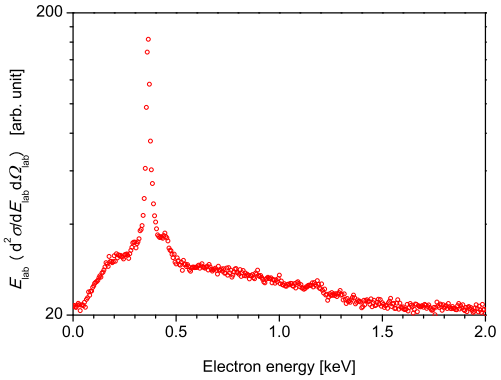

Fig. 1. Energy spectrum of zero degree electrons induced by the irradiation of 16 MeV C_2^+ ions through 3 μg/cm^2 carbon foil.

Table 1. Relative electron yield from 3μg/cm^2 carbon foil. The yields are normarilzed with that of projectile KLL Auger electrons.

	Convoy electron	Coster-Kronig	Binary electon
$Y\left(C_2^+\right)/Y\left(C^+\right)$	4.3	2.3	0.8

References

[1] H. Rothard, et. al., Phys. Rev. A **41**, 2521 (1990).

[2] S. Tomita et. al., Phys. Rev. A **82**, 044901 (2010)

[3] S. Tomita et. al., Phys. Rev. A **73**, 06901 (2006).

[4] K. Kawatsura et al., Nucl. Instr. and Meth. in Phys. Res. B **53**, 421(1991).

[5] R. Bruch, et. al., Phys. Rev. A, **31**, 310 (1985).

[6] Y. Yamazaki et. al., Phys. Rev. Lett. **57**, 992(1986).

3.2 Coincidence measurement of secondary electrons with scattered ions under irradiation of fast carbon-cluster ions

Y. Shiina, R. Kinoshita, S. Tamura, K. Sasa, S. Ishii and S. Tomita

The swift atomic ion penetrate bulk material with losing its kinetic energy by producing scattered electrons, and inducing wake potential. As a result of the energy transfer, secondary particles (electrons and sputtered atoms), and photons are produced and modification of the target materials might be caused depending on the target and injected ions. If two or more atomic ions are injected simultaneously, the physical process might be different from the case of atomic ion injection. Because the volume affected by atomic ion might have overlap, if the atomic distances between injected ions are close enough. This kind of physical process might take place when we inject fast cluster ions, such as C_n^+. This is called cluster effect, and have been observed in many cases such as the yield of secondary ions, sputtering yield, stopping powers, equilibrium charge state, etc.

Among these phenomena, we investigated in the cluster effect of secondary electron yield. Because swift ions mainly loses its kinetic energy through electronic stopping power, the behavior of secondary electrons in the target material might be most important process to understand the cluster effects. We have actually reported strong cluster effect on the secondary electron yield. Secondary electron yield per number of incident atom for 0.5 MeV/atom C_4^+ ion is almost 50% of that of atomic ion with same velocity, while the electronic stopping power of C_4^+ is almost same as that of four atomic ions[3].

The mechanism of secondary electron emission can be understood as three step process. Scattered electrons are produced inside target material through scattering process by projectile ions (production). The scattered electrons move inside material, and some of them are transported to the bulk surface (transport). A part of these electrons transmit from target surface overcoming ionization potential (transmission). Since the cluster effect on the stopping power is weak compared to that of secondary electron yield. It seems that the secondary electron suppression mechanism should be attributed either to the transport of scattered elections inside material or transmission process through the material surface, rather than the production process.

To investigate this problem further, we have studied the cluster effect of secondary electron, which produced by close distant collisions. It is known that the secondary electron yield is higher for the close distance collision. Therefore, we measured the correlation of secondary electron emission with the number of scattered atoms in solids. The schematic setup is shown in figure 1. A SSD is located in forward angle. The ions emitted in small angle (smaller than 3 degrees) are detected by SSD. The pulse height of SSD signal is proportional to the number of atomic ion detected at the same time, thus, the number of scattered atom can be determined. The secondary electron yield in backward angle is measured with MCP, in coincidence with the SSD signal.

Average of secondary electron yields as a function of the number of scattered atoms is shown in figure 2. The more atoms were scattered the more secondary electrons were emitted. It should be noted that the increase of secondary electron yields was almost linear to the number of scattered atoms. The linearity

implies that the increase is mainly attributed to the result of close distant collision. It is reported by Ogawa et al. [4] for H^+ ions that the wider the scattering angle was, the more secondary electrons were emitted. We are planning to measure secondary electron yields by incident of atomic ions to compare with present result. The comparison allows us to evaluate suppression effect of scattered elections from close distant collisions. If the suppression effect is as same as that of secondary electrons, this might be one of experimental evidence that prove independence of the suppression mechanism from the production process of scattered electrons.

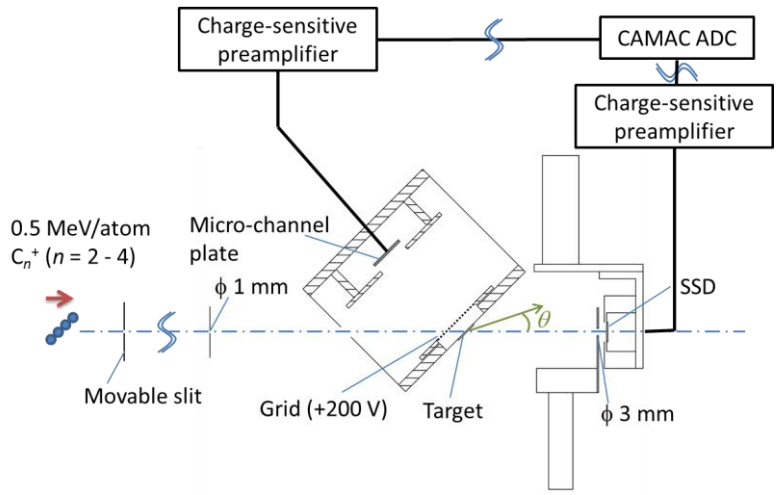

Fig. 1. Schematic setup

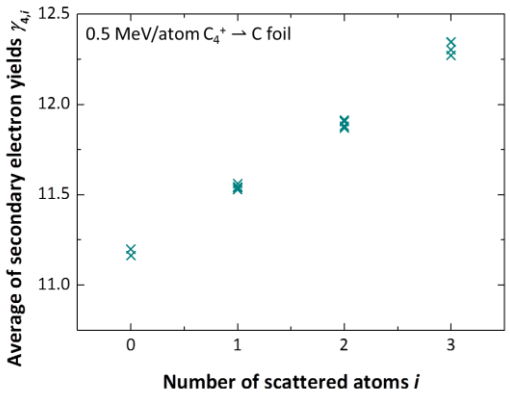

Fig. 2. Average of secondary electron yields as a function of the number of scattered atoms

References

[1] H. Rothard, K. Kroneberger, A. Clouvas, E. Veje, P. Lorenzen, N. Keller, J. Kemmler, W. Meckbach, and K. O. Groeneveld, Phys. Rev. A 41, 5 (1990).

[2] H. Arai, H. Kudo, S. Tomita, and S. Ishii, JPSJ. 78 (2009) 104301.

[3] S. Tomita, M. Murakami, N. Sakamoto, S. Ishii, K. Sasa, T. Kaneko, and H. Kudo, Phys Rev. A 82, 044901 (2010).

[4] H. Ogawa, H. Tsuchida and N. Sakamoto, Phys. Rev. A 68, 052901 (2003).

3.3 Detection of vacancy-type defects in $In_xGa_{1-x}N$ alloys using a monoenergetic positron beam

T. Watanabe, A. Uedono, S. Ishibashi[1], X. Q. Wang[2], S. T. Liu[2], G. Chen[2], L. W. Sang[3], M. Sumiya[3], and B. Shen[2]

Introduction

Group III nitrides, along with their alloys, have been extensively studied because of their potential for device applications such as light-emitting diodes, laser diodes, photo-detectors, and high electron mobility transistors used in high-power and high-speed electronics. For $In_xGa_{1-x}N$ wurtzite alloys, cation sites are randomly occupied by In or Ga atoms, where the difference between GaN and InN bond lengths is roughly 11%. Thus, the positions of atoms could fluctuate from the resulting stress, and this may lead to not only compositional inhomogeneity but also to the introduction of dislocations and point defects. Because such defects are known to closely relate to the optical and electrical properties of group-III nitrides, knowledge of defect behaviors is crucial for the development of $In_xGa_{1-x}N$-based devices. Positron annihilation is a powerful technique for evaluating vacancy-type defects in semiconductors [1]. The studies of defects in group-III nitrides have been systematically performed, and the results show that positrons are a powerful probe for studying vacancies and vacancy complexes with impurities. In this report, we have used monoenergetic positron beams to probe native cation vacancies in $In_xGa_{1-x}N$ grown by plasma-assisted MBE.

When a positron is implanted into condensed matter, it annihilates with an electron and emits two 511-keV γ quanta [1]. The energy distribution of the annihilation γ rays is broadened by the momentum component of the annihilating electron-positron pair, which is parallel to the emitting direction of the γ rays. A freely diffusing positron may be localized in a vacancy-type defect because of Coulomb repulsion from positively charged ion cores. Because the momentum distribution of the electrons in such defects differs from that of electrons in the bulk material, these defects can be detected by measuring the Doppler broadening spectra of the annihilation radiation. The resultant changes in the spectra are characterized by the *S* parameter, which mainly reflects changes due to the annihilation of positron-electron pairs with a low-momentum distribution. In general, the characteristic value of *S* expected for the annihilation of positrons due to their trapping by vacancy-type defects is larger than that for positrons annihilated from the free-state. For group-III nitrides, because an isolated nitride vacancy (V_N) is positively charged, the major trapping center of positrons is cation monovacancies such as In vacancy (V_{In}) and Ga vacancy (V_{Ga}) or their complexes such as $V_{In}V_N$ and $V_{Ga}V_N$.

Experiment

The samples investigated were 200-600 nm thick $In_xGa_{1-x}N$ ($0.05 \le x \le 0.90$) grown on GaN/sapphire

[1] Nanosystem Research Institute "RICS", National Institute of Advanced Industrial Science and Technology, Tsukuba, Japan
[2] School of Physics, Peking University, China
[3] Wide Bandgap Material Group, National Institute for Materials Science, Tsukuba, Japan

templates using plasma-assisted MBE. The growth method and the optical properties of samples prepared by this method are described elsewhere [2]. The InN fractions were determined by using x-ray diffraction (XRD) reciprocal space mapping. Photoluminescence (PL) spectra were measured with a 325-nm He-Cd laser as an excitation source and a Perkin-Elmer Lambda 950 UV-Vis-NIR spectrophotometer. All measurements were made at room temperature. For comparison, MBE-grown InN ($n_e = 5\times10^{17}$ cm^{-3}) was also characterized. Details of the growth conditions and properties of InN are described elsewhere [3].

With a monoenergetic positron beam, the Doppler broadening spectra of the annihilation radiation were measured with a Ge detector as a function of the incident positron energy E. Doppler broadening profiles with 5×10^6 counts were then measured using a coincidence system. The low-momentum part was characterized by the S parameter, defined as the number of annihilation events over the energy range of 511 keV $\pm \Delta E_\gamma$ (where $\Delta E_\gamma = 0.76$ keV) around the center of the peak.

Doppler broadening spectra corresponding to the annihilation of positrons in the delocalized (defect-free) state and the trapped by typical vacancies in ordered $In_{0.5}Ga_{0.5}N$ were theoretically calculated using our in-house QMAS (Quantum MAterials Simulator) code, which uses valence-electron wavefunctions determined by the projector augmented-wave (PAW) method.

Results and Discussion

Figure 1 shows the S values of $In_xGa_{1-x}N$ (x =0.36, 0.44, and 0.90) grown using plasma-assisted MBE as a function of incident positron energy E. The S–E curves for InN grown by plasma-assisted MBE and GaN grown by hydride vapor phase epitaxy (HVPE) are also shown. For HVPE-GaN, the observed increase in the S values at low E (≅ 0.1 keV) is associated with the annihilation of positrons at the surface, and those above E = 20 keV correspond to the annihilation of positrons in the films, where the bulk S value ($E \geq 20$ keV) was close to that previously reported for defect-free HVPE-GaN [4]. For $In_xGa_{1-x}N$ and InN, the decrease in the S value at high E (> 10 keV) can be attributed to the annihilation of positrons in the GaN/sapphire template. For $In_xGa_{1-x}N$ (x =0.36, 0.44, and 0.90), the S value observed at E = 3-7, 4-5 and 4-10 keV corresponds to the annihilation of positrons in the $In_xGa_{1-x}N$ film, respectively. For InN, the S value tends to saturate at E = 10 ~ 15 keV, suggesting the annihilation of positrons in the InN film. For this sample, the S values at E ≅ 20 keV were higher than the saturated S value, suggesting the annihilation of positrons by vacancy-type defects near the InN/GaN interface. Similar behavior of the S values was also observed for $In_xGa_{1-x}N$, and this is typical for group-III nitride films grown by heteroepitaxial growth [4].

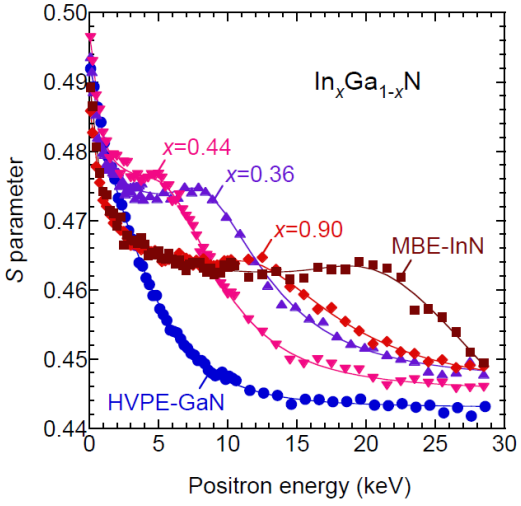

Fig.1. S parameters as a function of incident positron energy E for $In_xGa_{1-x}N$ (x = 0.36, 0.44, and 0.90), InN, and GaN.

Figure 2 shows (a) the FWHM (full-width at half maximum) values of XRD ω-rocking curves for (002) and (102), (b) the line-width (FWHM) of PL lines [2], and (c) the *S* values for $In_xGa_{1-x}N$ as a function of In composition *x*. It can be seen that the FWHMs for both (002) and (102) tend to increase with increasing *x*, suggesting a decrease in the crystal quality for In-rich $In_xGa_{1-x}N$. The line-width of the PL peaks also broadened with increasing *x*, and reached the maximum at the mid-In composition. The observed increase in the FWHM values of XRD and PL intensity can be associated with the alloy disorder or compositional inhomogeneity caused by the increase in the strain energy [2].

More details and other results of these measurements are described elsewhere [5].

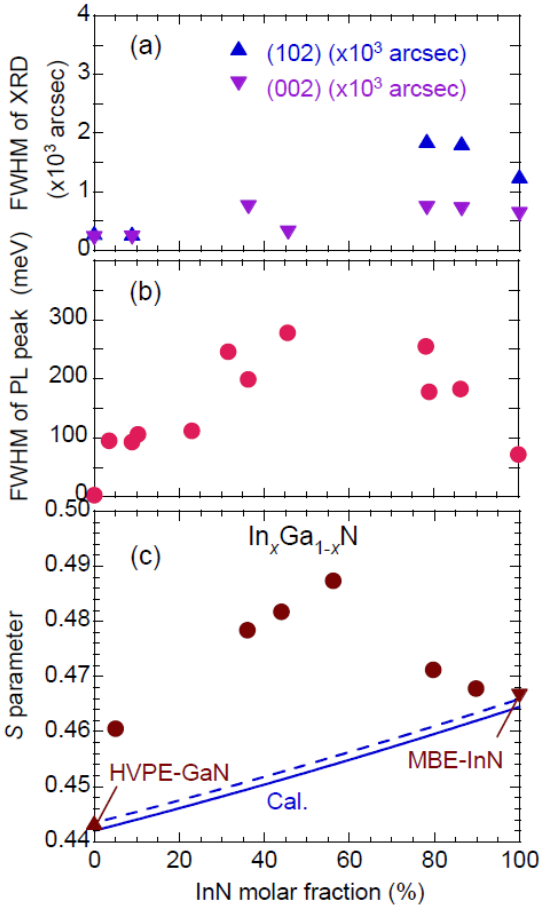

Fig.2. (a) FWHM values of XRD ω-rocking curves for (002) and (102), (b) FWHM values of PL peak [2] and (c) *S* values of $In_xGa_{1-x}N$ as a function of the In molar fraction *x*. In (c), the calculated *S*–*x* relationship (solid curve marked as Cal.) for defect-free $In_xGa_{1-x}N$ and the shifted one (broken curve) are also shown.

Summary

We studied vacancy-type defects in $In_xGa_{1-x}N$ grown by plasma-assisted MBE using a monoenergetic positron beam. Doppler broadening spectra were measured as a function of the incident energy of positrons for 200-600 nm thick $In_xGa_{1-x}N$ grown on GaN/sapphire templates. Coincidence Doppler broadening spectra were also measured, and those were compared with the results calculated using the PAW method. The concentration of vacancy-type defects increased with increasing In composition *x*, and reached the maximum at $x = 0.44 \sim 0.56$. A clear correlation between the line-width of PL and the concentration of vacancy-type defects was obtained.

References

[1] R. Krause-Rehberg *et al*., Positron Annihilation in Semiconductors, Solid-State Sciences (Springer-Verlag, Berlin, 1999) vol. 127.

[2] S. T. Liu *et al*., J. Appl. Phys. **110**, 113514 (2011).

[3] X. Q. Wang *et al*., Appl. Phys. Express. **5**, 015502 (2012).

[4] A. Uedono *et al*., J. Appl. Phys. **103**, 104505 (2008).

[5] A. Uedono *et al*., J. Appl. Phys. **112**, 014507 (2012)

3.4 Site population of Fe ions in Mg-containing Fe_3O_4 nanoparticles determined by Mössbauer spectroscopy

D. Isaka, M. Kishimoto, H. Yanagihara, E. Kita

Magnetic nanoparticles have attracted much attention because of their potential to generate heat in magnetic hyperthermia and thermoablation for cancer therapy. We have studied ferromagnetic nanoparticles, especially cobalt-doped magnetite particles, as high heat-generating materials for magnetic hyperthermia and thermoablation [1]. In addition to the high heating ability, the biocompatibility of magnetic materials must be considered for their practical use. The biocompatibility of elements other than iron, cobalt in particular, needs to be carefully checked, even when they are used as dopants. Therefore, we have synthesized Mg-containing iron oxide particles and reported their magnetic properties[2] because Mg is believed to be a safe element. To obtain high heating ability, the magnetic properties of nanomagnets need to be controlled precisely. For spinel ferrites, the site population of divalent elements, Mg in the present case, determines the magnetic properties. In the present study, the site preference of Fe ions on the spinel structure, which is closely connected to their influence on the magnetic properties, was investigated with a Mössbauer study.

Spinel-structured Mg-containing iron oxide nanoparticles, $(Mg)Fe_3O_4$, were synthesized by coprecipitation and a hydrothermal process. We have labeled the various nanoparticle samples MTH0 (pure Fe_3O_4) through MTH6, corresponding to the increasing Mg content from 0 to 10.0 at% with respect to the total Fe content: the 10 at% concentration corresponds to $Mg_{0.33}Fe_{2.67}O_4$. The magnetization of dry powdered samples was measured using a vibration sample magnetometer (VSM). The particle size and crystal structure were obtained using X-ray diffraction (XRD). Mössbauer spectra were recorded at 77 K and were numerically analyzed using commercially available fitting software, MössWinn 4.0.

The basic characteristics of the $(Mg)Fe_3O_4$ particles in the various samples are summarized in Table I. The magnitude of the coercive forces peaked for the MTH1 sample and then decreased with increasing Mg content.

Table I. Characteristics of $(Mg)Fe_3O_4$ particles.

Sample	Mg content at%	D_{XRD} (nm)	H_c (Oe)	M_s (emu/g)
MTH0	0	41	141	85
MTH1	2.0	33	155	77
MTH2	3.2	24	136	70
MTH3	4.0	21	109	68
MTH4	6.0	18	71	63
MTH5	8.0	15	41	54
MTH6	10.0	14	40	51

Figure 1 shows the Mössbauer spectra of $(Mg)Fe_3O_4$ particles recorded at 77 K. The solid lines indicate the fitted results. For all samples, the spectra were composed of three ferromagnetic subspectra, which correspond to those from Fe_3O_4. The fitted results are summarized in Table II. The subspectrum with the highest hyperfine field (H_{hp}), about 515 kOe, is attributed to the Fe^{3+} ions in octahedral sites (B sites), and that with the second largest hyperfine field (H_{hp}), 507 kOe, to tetrahedral sites (A sites). The smallest one,

470-480 kOe, corresponds to the Fe^{2+} ions in the octahedral sites (B sites). Compared with room temperature spectra, the subspectra from $Fe^{2.5+}$ ions disappeared due to the electronic charge order, namely, Verwey transition, and traces of the superparamagnetism were not detected at 77 K, suggesting that superparamagnetic parts were ordered magnetically at this temperature. The populations of Fe^{2+} and Fe^{3+} on the B sites in the spectrum for MTH0 without Mg is not identical to those of bulk and slightly different.

The distribution can be estimated from the area ratios of the subspectra summarized in Table II. To determine the occupation, Mössbauer analyses were generally performed at 77 K. Mg atoms tend to occupy B sites in the thin Mg concentration region below $Mg_{0.5}Fe_{2.5}O_4$ [3]. The concentration of Mg atoms in this study is thinner than that found in previous research. As seen in Table 1, the relative ratio of Fe^{2+} ions tends to decrease with increasing Mg content. This is reasonably explained by the increase in the occupation of Mg ions at B sites in this concentration range.

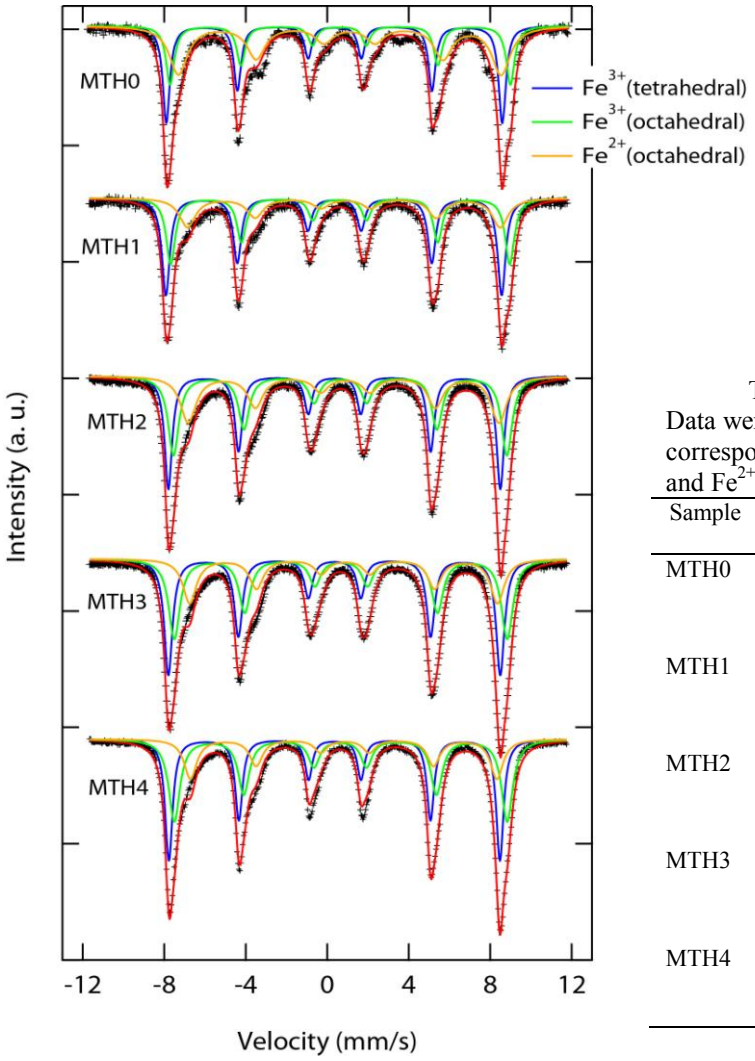

Table II. Mössbauer fitting parameters
Data were recorded at 77 K. 3A, 3B, and 2B sites correspond to Fe^{3+} ions at A sites, Fe^{3+} ions at B sites, and Fe^{2+} ions at B sites, respectively.

Sample	ion	H_{hf} (kOe)	IS (mm/s)	QS (mm/s)	P (%)
MTH0	3A	513	0.359	-0.022	33.0
	3B	519	0.621	-0.043	23.1
	2B	492	0.856	-0.481	41.8
MTH1	3A	512	0.342	-0.037	41.1
	3B	517	0.626	0.030	32.0
	2B	477	0.863	-0.090	24.8
MTH2	3A	507	0.353	-0.013	34.4
	3B	509	0.642	-0.013	34.4
	2B	474	0.846	-0.088	29.0
MTH3	3A	507	0.355	-0.010	37.9
	3B	508	0.674	-0.021	35.7
	2B	470	0.853	-0.093	23.7
MTH4	3A	505	0.360	-0.018	38.5
	3B	508	0.650	0.025	39.8
	2B	468	0.836	-0.061	21.7

References

[1] E. Kita *et al.*, J. Phys. D: Appl. Phys. **43** (2010) 474011.

[2] D. Isaka, M. Kishimoto, H. Yanagihara, and E. Kita, UTTAC ANNUAL REPORT 2011 (2012) 20.

[3] F. Nakagomi *et al.*, J. Solid State Chem. **182** (2009) 2423.

3.5 Development of ΔE-E telescope ERDA detector

I. Harayama, K. Nagashima, Y. Hirose[1], H. Oikawa, R. Akiyama, S. Kuroda, H. Matsuzaki[2], D. Sekiba

Recently the materials designs including light elements are intensively suggested in the various fields, such as lithium (Li), carbon (C), nitrogen (N), oxygen (O) and fluorine (F). In particular, the N- or F-doped metal oxides have been well studied from the viewpoint of the solar-cell and battery, etc. In the case of synthesizing new materials, it is generally important to determine the accurate concentration of each element. However the estimation of the concentration is not straightforward, when the materials contain several light elements. In this case, elastic recoil detection analysis (ERDA) using heavy ions is effective. Especially, the ΔE-E telescope ERDA using ionization chamber and/or time-of-flight (TOF) ERDA are better tools for the particle identification. Here we present our recent development of the ΔE-E telescope ERDA detector, which can be constructed without expensive parts [].

We adopted the simple combination of the ionization chamber and the Si surface detector (SSD) as schematically shown in Fig. 1. In the concept of the design of the ionization chamber, we focused our chief attention onto the identification of O and N recoiled by 40 MeV chlorine ion ($^{35}Cl^{7+}$). The PR gas (90% Ar + 10% CH_4) is adopted for the ionization chamber, and the pressure of the PR gas is fixed at 6000 Pa. From some literatures, we estimate the energy resolution of the ionization chamber as in principle about ~ 100 keV. Therefore, the difference of the energy loss ΔE of O and N in the ionization chamber should be 400 ~ 500 keV to identify them. By means of the SRIM calculation [2], we set the length of the ionization chamber along the beam direction as 50 mm. The electric potentials of the cathode, Frisch grid and the anode are set at 0 V, 30 V and 180 V, respectively. These values are referred from the literature of accelerator mass spectroscopy (AMS). All the setup is compactly mounted on the single ICF152 flange, and the gas chamber is separated from the vacuum chamber by the mylar film with 3.5 μm thickness.

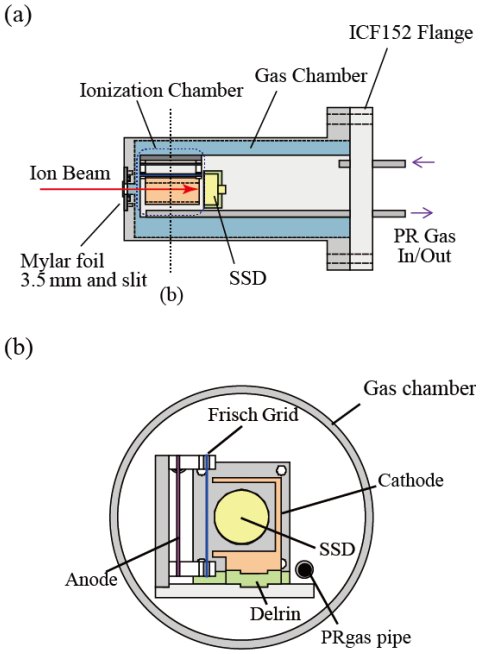

Figure 1. The schematic drawings of the ionization chamber: a top view of the gas chamber (a) and a cutaway view seen from a front of the ionization chamber (b).

Figure 2 (a) ~ (d) display the two-dimensional maps (2D map) of ΔE and E_{res} taken on (a) $CoON/MgAl_2O_4$, (b) $LiTaO_3$ (bulk sample), (c) $InOF/ZrO_2$ and (d) SiO_2/Si by using the developed ΔE-E telescope detector. The recoil angle is 30 degree from the beam direction. Here, Eres is the energy of

[1] Graduate School of Science, The University of Tokyo, 7-3-1 Hongo, Bunkyo-ku Tokyo 113-0033, Japan
[2] School of Engineering, The University of Tokyo, 7-3-1 Hongo, Bunkyo-ku Tokyo 113-8656, Japan

particle measured on SSD, and $\Delta E + E_{res} = E_{total}$. We can see that the various light elements Li, C, N, O and F are well distinguished on the maps. Some light metals, such as Al and Mg are separately observed beside the intense signals of forward scattered Cl ions. Finally, we also put another SSD to detect the backscattered particles in the direction of 150 degree from the beam direction, so that we can determine the whole elemental concentration of materials, which include the both heavy metals and light elements.

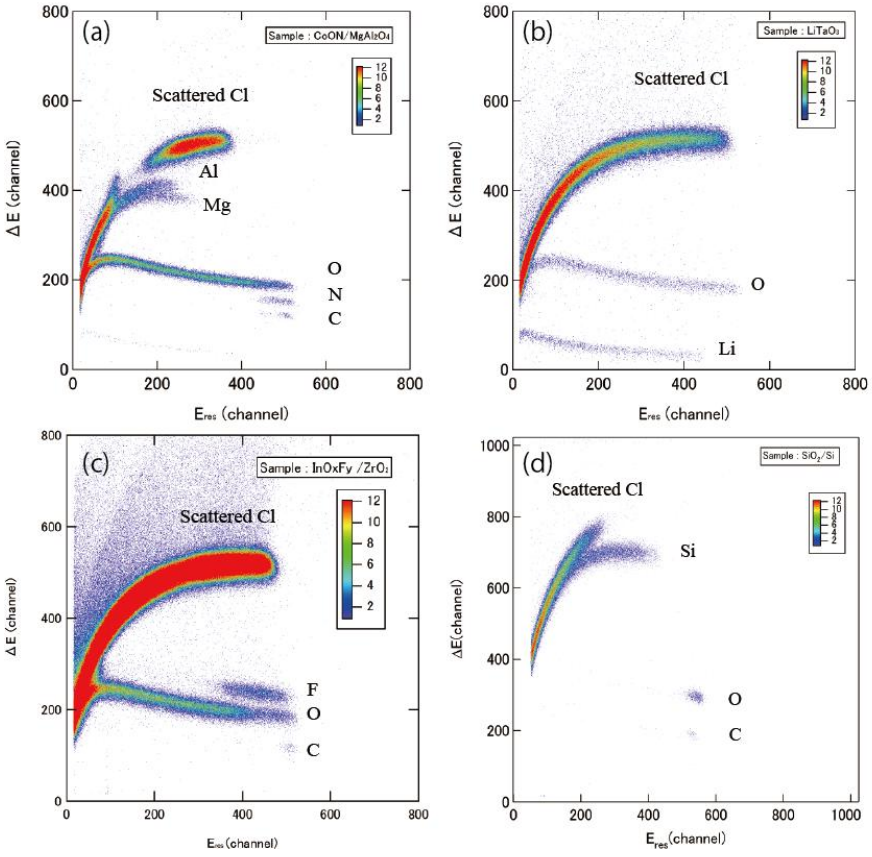

Figure 2. The ΔE-E_{res} two dimensional maps taken on (a) $CoON/MgAl_2O_4$, (b) $LiTaO_3$ (bulk sample), (c) $InOF/ZrO_2$ and (d) SiO_2/Si. Here, E_{res} stands for the energy measured by SSD. $\Delta E + E_{res}$ is equal to E_{total} of the recoiled or forward scattered particles.

References

[1] J.P.Stoquert, G. Guillaume, M. Hage-ali, J.J. Grob, C. Ganter and P. Siffert. Nucl. Instr. and Meth. B**44**(1989)184-194.

[2] SRIM2013, http://www.srim.org.

4.

ACCELERATOR MASS SPECTROMETRY

4.1 Distribution of iodine 129 from the Fukushima No. 1 nuclear power plant accident

K. Sasa, K. Sueki, T. Takahashi, M. Matsumura, Y. Satou, S. Abe, N. Kinoshita[1] and H. Matsuzaki[2]

A tremendous amount of radioactivity was discharged due to the damage to cooling systems of nuclear reactors in the Fukushima No.1 nuclear power plant in March 2011. Fukushima and its adjacent prefectures were contaminated with fission products from the accident. We measured short-lived radionuclides such as ^{129m}Te, ^{131}I, ^{134}Cs, ^{136}Cs and ^{137}Cs in the surface soils immediately after the accident at Fukushima and the Kanto area [1]. Figure 1 shows geographical distributions of radioactive iodine, tellurium, and cesium in surface soils of central-east Japan as determined by gamma ray spectrometry.

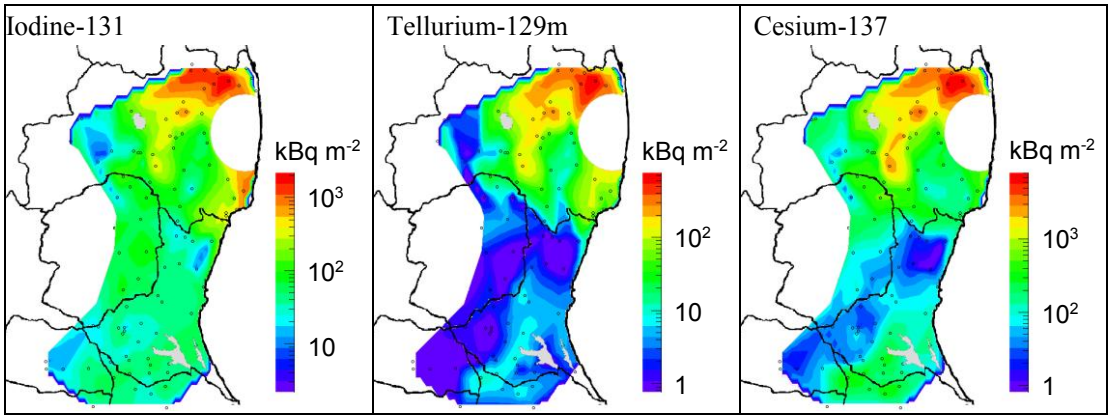

Figure 1. Geographical distribution of ^{131}I, ^{129m}Te and ^{137}Cs on 29 March, 2011 [1].

Radioactive iodine is one of the most important radionuclides released from the Fukushima No. 1 nuclear power plant accident. ^{131}I has a short half-life time of about 8 days. Because of the difficulty of measuring ^{131}I at this time, it is expected to estimate ^{131}I precipitation from ^{129}I with a long half-life time of 1.57×10^7 years. We have measured ^{129}I concentrations in surface soils that we already got results of ^{131}I concentrations. ^{129}I/^{127}I ratios were measured by accelerator mass spectrometry (AMS) at MALT, The University of Tokyo [2]. Stable iodine of ^{127}I was determined by inductively coupled plasma mass spectrometry (ICP-MS). We got a result that the average ^{129}I concentration was about 0.41 mBq/kg prior to the Fukushima No. 1 nuclear power plant accident as ^{129}I background at the eastern area of Fukushima Prefecture. After the accident, average isotopic ratio of ^{129}I/^{131}I is estimated to 26.0 ± 5.6 as at 11 March 2011. ^{129}I and ^{131}I has a good linear correlation, it is therefore possible to reconstruct ^{131}I distribution from ^{129}I analysis in the future. Figure 2 shows the distribution of ^{129}I precipitation from the Fukushima No. 1 nuclear power plant accident at the eastern area of Fukushima Prefecture.

[1] Shimizu Co.
[2] MALT, The University of Tokyo

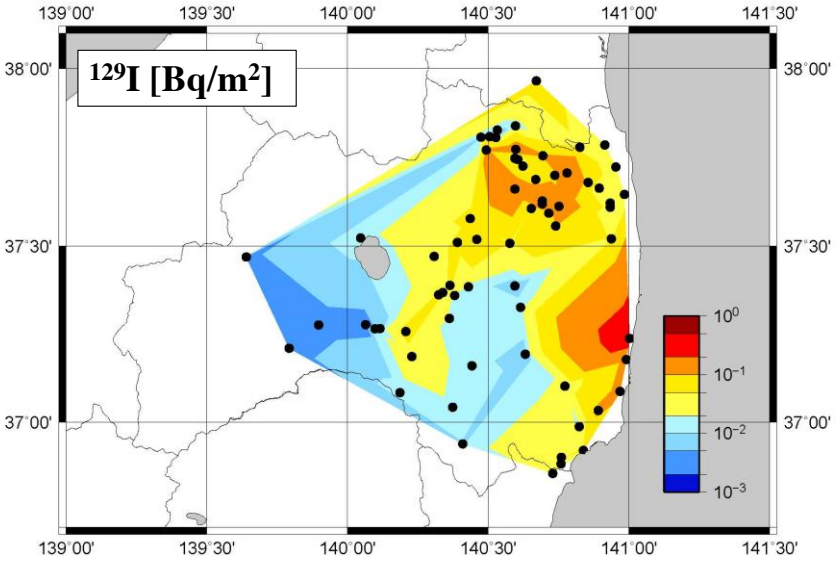

Figure 2. Distribution of ^{129}I precipitation from the Fukushima No. 1 nuclear power plant accident at the eastern area of Fukushima Prefecture as of March 2011.

Acknowledgements

This work was supported by JSPS KAKENHI Grant Numbers 24246156 and 24110006, and Reconstruction support program for eastern Japan at the University of Tsukuba.

References

[1] Norikazu Kinoshita, Keisuke Sueki, Kimikazu Sasa et al., *PNAS*, 108 (2011) 19526-19529.

[2] Hiroyuki Matsuzaki et al., *Nucl*. *Instr*. *Meth*. *Phys*. *Res*. B 259, (2007) 721-726.

5.

INTERDISCIPLINARY RESEARCH

5.1 Comparison of calibration curves for a new and old Si (Li) detectors with different energy resolution

M. Kurosawa, K. Sasa and S. Ishii

Introduction

Reliable calibration factors or sensitivities of Si(Li) X-ray detector (expressed in counts/μg/cm^2/μC or cts/μg/g/μC) are important for PIXE quantification. The factors, including solid angle and detection efficiency of the detector, have been usually determined based on measurements of X-ray yields from thin-film or solid reference materials with known compositions [1-7]. The thin-film reference materials are fragile, sometimes impure, and the thicknesses are uncertain by ±5−10% [2]. Thus, the solid reference materials are advantageous in case that suitable correction for energy loss of incident beams and self-absorption of generated X-rays in matrix are performed for the X-ray yields [2]. In this report, we have determined the sensitivities by using solid reference materials to compare the analytical capability of a newly equipped Si(Li) X-ray detector with higher energy resolution and that of old detector with lower energy resolution in the PIXE facility installed on 1-MV Tandetron accelerator at the Tandem Accelerator Complex, University of Tsukuba.

Reference materials

The detector sensitivities for each element were determined by using three multielement reference glass materials (NIST SRM 1412 and 1873), two mineral reference materials, and thirteen synthetic crystals for semiconductor and optical devices (Table 1). Elemental contents in the reference materials were selected from the certified values for the reference glass materials and the mineral references, and those in the synthetic crystals were adopted from the stoichiometric compositions. Pieces of each material, about 3 mm × 3 mm × 2 mm, were mounted on a glass slide with resin and then were cut and polished. The specimens were coated with a carbon film to prevent electrostatic charging and to measure the integrated charges.

Table 1. Reference materials

Sample	Composition*	Maker#
SRM 1412	reference glass material*	NIST
SRM 1873 K-489	reference glass material*	NIST
SRM 1873 K-963	reference glass material*	NIST
$KTiOPO_4$	synthetic crystal	POE
Apatite	natural mineral reference*	MAC
Cr_2O_3	synthetic crystal	NCL
NiO	synthetic crystal	NCL
$SrTiO_3$	synthetic crystal	POE
$Y_3Al_5O_{12}$	synthetic crystal	POE
Zircon	natural mineral reference*	MAC
$LiNbO_3$	synthetic crystal	UO
$AgGaS_2$	synthetic crystal	POE
InP	synthetic crystal	POE
$LaAlO_3$	synthetic crystal	NCL
$Gd_3Ga_5O_{12}$	synthetic crystal	ELAN
$LiTaO_3$	synthetic crystal	NCL
$CdWO_4$	synthetic crystal	MT
$PbMoO_4$	synthetic crystal	POE

*Composition: SRM1412: mixed glass of Li, B, Na, Si, Mg, K, Ca, Zn, Sr, Cd, Ba, and Pb oxides; K-489: Ba-Zn silicate glass with minor Ti, Fe, Zr, Ba, Ce, Ta, and Pb; K-963: Ba-Zn silicate glass with minor P, Cr, Ti, Ni, Ge, Zr, Ba, Eu, Th, and U; Apatite: $Ca_5(PO_4)_3(F,Cl,OH)$; Zircon: $(Zr,Hf)SiO_4$.
#NIST: National Institute of Standards and Technology, U.S.A; POE: Phiscience Opto-electronics CO., Ltd., Beijing, China; MAC: Micro-Analysis Consultants Ltd., Cambridgeshire, U.K; NCL: Nakazumi Crystal Laboratory, Osaka, Japan; UO: Unioriental Optics Co., Ltd., Beijing, China; ELAN: ELAN Ltd., Saint-Petersburg, Russia; MT: MolTech GmbH, Berlin, Germany.

Experimental

PIXE analyses were performed at the 1MV Tandetron. A 1.92-MeV proton beam was focused to a 33 x 33 μm spot on the specimens. The beam

incidence was normal to the specimen surface, and the X-ray measurement take-off angle was 45°. The characteristic X-rays were simultaneously collected by the new and old Si(Li) X-ray-energy detectors (Fig. 1). The new detector (Sirius 30+ detector, e2V Scientific Instruments, UK) had the area of the detector of 30 mm^2, and the energy resolution was 137 eV at 5.9 keV. The old detector (Sirius detector, Gresham Scientific Instruments, UK) had the area was 50 mm^2, and the resolution was 155 eV at 5.9 keV. The energy resolutions were determined by measurements of Mn impurities in a mineral willemite. The sample-to-detector distances were 2.5 cm for both detector, and a 55-μm-thick Mylar filter was placed between the specimen and both detector. The X-ray spectra were recorded by a multichannel analyzer. The beam current was set at 0.05–0.25 nA to obtain good counting statistics. The total charge was determined by integrating the target currents, and all specimens were analyzed at integrated charges of 0.03 to 0.71 μC. A suppressor electrode was placed near the sample surface to prevent loss of integrated charge by secondary electron emission from insulating matrices. The detector sensitivities were calculated based on the method by Kurosawa et al [8]. In the calculations, L X-ray production cross sections for Sr, Y, Zr, Nb, and Mo were estimated from interpolations for data of Orlic et al [9] and Reis and Jesus [10].

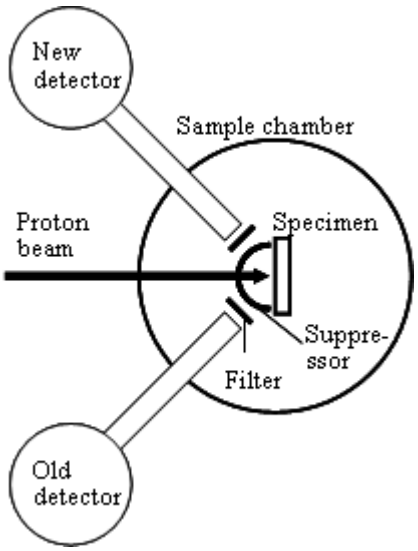

Fig.1. Schematic drawing of the sample chamber in the PIXE facility. The incident proton beam and the detector angles are at 90° and 135°, respectively, to the specimen surface.

Results and Discussion

At the PIXE measurements, we observed K X-ray peaks from Si, P, S, Cl, K, Ca, Ti, Cr, Fe, Ni, Zn, Ga, Ge, Sr, Y, Zr, Nb, and Mo, and for L X-ray peaks from Sr, Y, Ze, Nb, Ag, Cd, In, Ba, La, Ce, Eu, Gd, Hf, Ta, W, Pb, Th, and U. Since the new detector had the higher energy resolution, it was possible to detect easily shoulder peaks of element of interest in the complex spectra generated by duplication of X-ray peaks from various elements (Fig. 2). In the spectrum of NIST SRM-1412 glass by the new detector, escape peaks of Cd and K on intense peak of Si, and a shoulder peak of Cd on intense peak of K were easily distinguished. A weak peak of trace Fe was also well shaped, indicating that the new detector is possible to

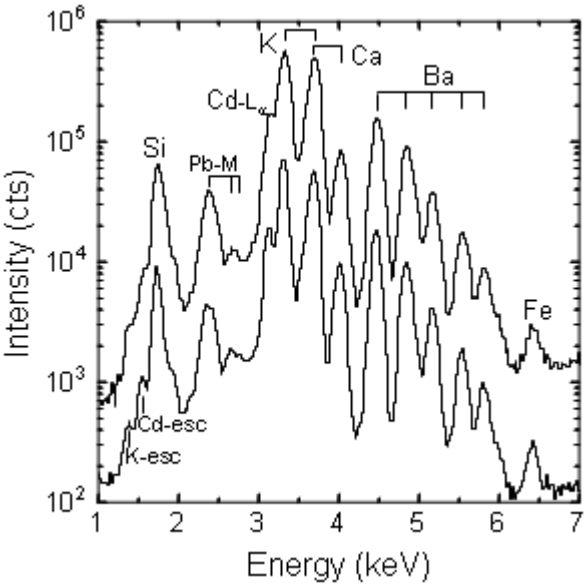

Fig.2. PIXE spectra of NIST SRM-1412 glass by the old detector (upper) and the new detector (lower). esc: escape peaks.

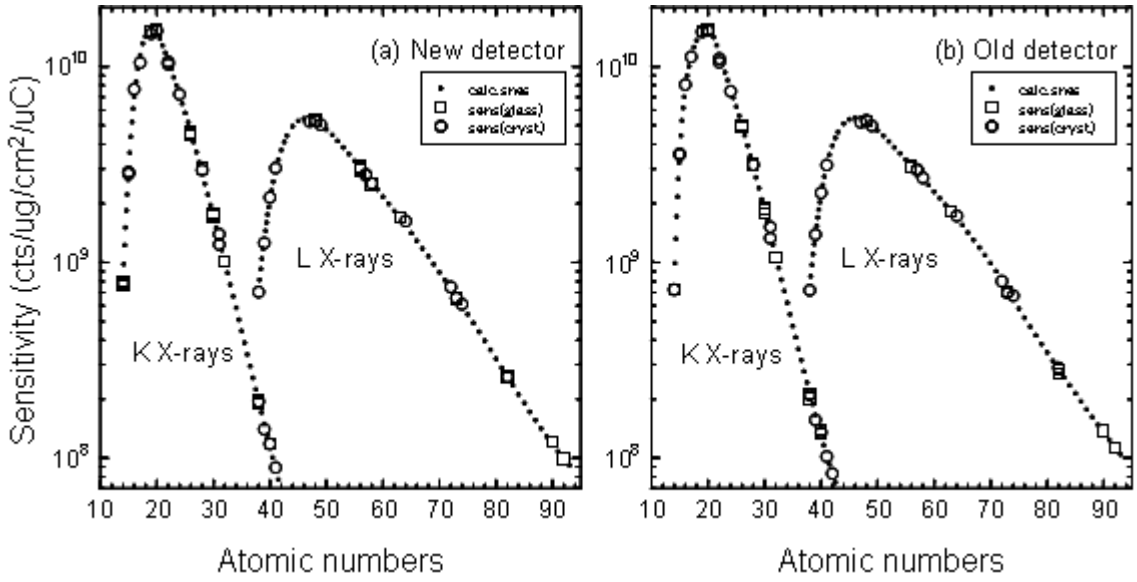

Fig.3. Detector sensitivities for K and L X-rays (1.92-MeV proton beam, 55 μm-thick mylar filter) of the new detector (a) and the old detector (b). The sensitivities were calculated from PIXE measurements of three reference glass materials (open squares) and fifteen synthetic and natural crystals (open circles). Small dots represent the curves fit to the reference-glass and crystal data.

analyze trace elements at the measurements of relatively lower intensities. Based on the measured intensities, we determined the sensitivities for the both detectors (Fig. 3). The most of elements were contained in more than one kind of specimens, so the sensitivities for each element were determined by an average of the values from the several specimens. The values from the different specimens were within a ±3% relative difference, indicating the appropriate corrections for difference of matrices. The sensitivities of the both detectors at each element were almost identical in spite of the smaller detector-area of the new detector (Fig. 3). Although a Si(Li) detector with smaller active area should represent basically lower sensitivities as shown in Watjen and Cave [5], the both detectors demonstrated the nearly same capabilities of X-ray detection. Thus, sensitive PIXE analyses with high energy-resolution can be expected by using the new detector.

References

[1] W. Maenhaut and H. Raemdonck, Nucl. Instr. Meth., B1 (1984), 123.

[2] J. L. Campbell et al., Nucl. Instr. Meth., B44 (1990), 347.

[3] M. Budnar et al., Nucl. Instr. Meth., B49 (1990), 138.

[4] I. Orlic et al., Nucl. Instr. Meth., B49 (1990), 166.

[5] U. Watjen and H. Cave, Nucl. Instr. Meth., B109/110 (1996), 395.

[6] S. Gama et al., Nucl. Instr. Meth., B181 (2001), 150.

[7] D. Cohen et al., Nucl. Instr. Meth., B189 (2002), 81.

[8] M. Kurosawa et al., Nucl. Instr. Meth., B266 (2008), 3633.

[9] I. Orlic et al., At. Data Nucl. Data Table, 56 (1994), 159.

[10] M. A. Reis and A. P. Jesus, At. Data Nucl. Data Table, 63 (1996), 1.

6. LIST OF PUBLICATIONS

The publications listed here are those released in the fiscal year 2012 by all the workers listed on p.52.

6.1 Journals

ACCELERATOR AND EXPERIMENTAL FACILITIES

1. A. Ozawa, T. Uesaka and M. Wakasugi, the Rare-RI Ring Collaboration, The rare-RI ring, Prog. Theor. Exp. Phys., 03C009 (2012).

2. Kimikazu Sasa, Damage Situation by the Great East Japan Earthquake and Post-quake Reconstruction Project of the Tandem Accelerator Facility at the University of Tsukuba, J. Particle Accelerator Society of Japan, Vol.**9**, No.1, 14-21 (2012).

NUCLEAR PHYSICS

3. K. Morita, K. Morimoto, D. Kaji, H. Haba, K. Ozeki, Y. Kudou, T. Sumita, Y. Wakabayashi, A. Yoneda, K. Tanaka, S. Yamaki, R. Sakai, T. Akiyama, S. Goto, H. Hasebe, M. Huang, T. Huang, E. Ideguchi, Y. Kasamatsu, K. Katori, Y. Kariya, H. Kikunaga, H. Koura, H. Kudo, A. Mashiko, K. Mayama, S. Mitsuoka, T. Moriya, M. Murakami, H. Murayama, S. Namai, A. Ozawa, N. Sato, K. Sueki, M. Takeyama, F. Tokanai, T. Yamaguchi, and A. Yoshida, New Result in the Production and Decay of an Isotope, 278113, of the 113th Element, J. Phys. Soc. Jpn., Vol.**81**, 103201 (2012).

4. D. Kameda, T. Kubo, T. Ohnishi, K. Kusaka, A. Yoshida, K. Yoshida, M. Ohtake, N. Fukuda, H. Takeda, K. Tanaka, N. Inabe, Y. Yanagisawa, Y. Gono, H. Watanabe, H. Otsu, H. Baba, T. Ichihara, Y. Yamaguchi, M. Takechi, S. Nishimura, H. Ueno, A. Yoshimi, H. Sakurai, T. Motobayashi, T. Nakao, Y. Mizoi, M. Matsushita, K. Ieki, N. Kobayashi, K. Tanaka, Y. Kawada, N. Tanaka, S. Deguchi, Y. Satou, Y. Kondo, T. Nakamura, K. Yoshinaga, C. Ishii, H. Yoshii, Y. Miyashita, N. Uematsu, Y. Shiraki, T. Sumikama, J. Chiba, E. Ideguchi, A. Saito, T. Yamaguchi, I. Hachiuma, T. Suzuki, T. Moriguchi, A. Ozawa, T. Ohtsubo, M. A. Famiano, H. Geissel, A. S. Nettleton, O. B. Tarasov, D. Bazin, B. M. Sherrill, S. L. Manikonda, and J. A. Nolen, Observation of new microsecond isomers among fission products from in-flight fission of 345 MeV/nucleon ^{238}U, Phys. Rev. C **86**, 054319 (2012).

5. S. Naimia, S. Nakamura, Y. Ito, H. Mita, K. Okada, A. Ozawa, P. Schury, T. Sonoda, A. Takamine, M. Wada, H. Wollnik, An rf-carpet electrospray ion source to provide isobaric mass calibrants for trans-uranium elements, Int. J. Mass Spectrom., **337**, 24–28 (2013).

6. H. Ueno, H. Miyatake, Y. Yamamoto, S. Tanimoto, T. Shimoda, N. Aoi, K. Asahi, E. Ideguchi, M. Ishihara, H. Izumi, T. Kishida, T. Kubo, S. Mitsuoka, Y. Mizoi, M. Notani, H. Ogawa, A. Ozawa, M. Sasaki, T. Shirakura, N. Takahashi, and K. Yoneda, β-delayed neutron and γ-ray spectroscopy of ^{17}C utilizing spin-polarized ^{17}B, Phy. Rev. C **87**, 034316 (2013).

7. Y. Ishibashi, D. Nagae, Y. Abe, T. Nagatomo, A. Ozawa, H. Suzuki, S. Fukuoka, R. Nishikiori, T. Niwa, K. Matsuta, Y. Tagishi, Production of nuclear polarization for unstable nucelai via polarization transfer reaction, Hyperfine Interaction , Proceedings of the 4th Joint International Conference on Hyperfine Interactions and International Symposium on Nuclear Quadrupole Interactions (HFI/NQI 2012),Beijing, China, 10–14 September 2012, http://rd.springer.com/article/10.1007/s10751-012-0750-0

8. T. Shizuma, T. Hayakawa, H. Ohgaki, H. Toyokawa, T. Komatsubara, N. Kikuzawa, T. Inakura, M. Honma, H. Nakada, Dipole strength distribution in ^{56}Fe, Phys. Rev. C **87**, 024301 (2013).

9. B. Ding, Y. H. Zhang, X. H. Zhou, G. X. Dong, F. R. Xu, M. L. Liu, G. S. Li, N. T. Zhang, H. X. Wang, H. B. Zhou, Y. J. Ma, Y. Sasakiz, K. Yamada, H. Ohshima, S. Yokose, M. Ishizuka, T. Komatsubara, K. Furuno, High-spin states in ^{127}I, Phys. Rev. C **85**, 044306 (2012).

10. B. Ding, H. X. Wang, H. Jiang, Y. H. Zhang, X. H. Zhou, Y. M. Zhao, S. T. Wang, M. L. Liu, G. S. Li, Y. Zheng, N. T. Zhang, H. B. Zhou, Y. J. Ma, Y. Sasaki, K. Yamada, H. Ohshima, S. Yokose, M. Ishizuka, T. Komatsubara, K. Furuno, High-spin level scheme of doubly odd ^{128}I, Phys. Rev. C **86**, 034302 (2012).

11. S. Kubono, N. B. Dam, S. Hayakawa, H. Hashimoto, D. Kahl, H. Yamaguchi, Y. Wakabayashi, T. Teranishi, N. Iwasa, T. Komatsubara, S. Kato, A. Chen, S. Cherubini, S. H. Choi, I. S. Hahn, J. J. He, H. K. Le, C. S. Lee, Y. K. Kwon, S. Wanajo, H.-T. Janka, Alpha-Cluster Dominance in the αp Process in Explosive Hydrogen Burning, Prog. Theor. Phys. (Kyoto), Suppl. **196**, 346 (2012).

12. J. J. He, L. Y. Zhang, A. Parikh, S. W. Xu, H. Yamaguchi, D. Kahl, S. Kubono, J. Hu, P. Ma, S. Z. Chen, Y. Wakabayashi, B.H. Sun, H.W. Wang, W. D. Tian, R. F. Chen, B. Guo, T. Hashimoto, Y. Togano, S. Hayakawa, T. Teranishi, N. Iwasa, T. Yamada, T. Komatsubara, Key ^{18}Ne(α, p) ^{21}Na breakout reaction in x-ray bursts: first experimental determination of spin-parities for α resonances in ^{22}Mg , via resonant elastic scattering of ^{21}Na + p, arXiv:1301.4283, (2013).

13. K. Setoodehnia, A. A. Chen, D. Kahl, T. Komatsubara, J.José, R. Longland, Y. Abe, D. N. Binh, J. Chen, S. Cherubini, J. A. Clark, C. M. Deibel, S. Fukuoka, T. Hashimoto, T. Hayakawa, J. Hendriks, Y. Ishibashi, Y. Ito, S. Kubono, W. N. Lennard, T. Moriguchi, D. Nagae, R. Nishikiori, T. Niwa, A. Ozawa, P. D. Parker, D. Seiler, T. Shizuma, H. Suzuki, C. Wrede, H. Yamaguchi, T. Yuasa, Nuclear

structure of ^{30}S and its implications for nucleosynthesis in classical novae, arXiv:1210.1194, (2012)

ACCELERATOR MASS SPECTROMETRY

14. Dong Kejun, Li Shizhuo, He Ming, Kimikazu Sasa, Yuki Matsushi, Huang Baojian, Ruan Xiangdong, Guan Yongjing, Tsutomu Takahashi, Keisuke Sueki, Li Chaoli, Wu Shaoyong, Wang Xianggao, Shen Hongtao, Yasuo Nagashima, Jiang Shan, Methodological study on exposure date of Tiankeng by AMS measurement of in situ produced cosmogenic ^{36}Cl, N. I. M. Phys. Res. B **294**, 611–615 (2013).

MATERIALS AND CLUSTER SCIENCE

15. K. Ozeki, D. Sekiba, T. Suzuki, K. Kanda, M. Niibe, K.K. Hirakuri, T. Masuzawa, Influence of the source gas ratio on the hydrogen and deuterium content of a-C:H and a-C:D films: Plasma-enhanced CVD with CH_4/H_2, CH_4/D_2, CD_4/H_2 and CD_4/D_2, Applied Surface Science **265**, 750-757 (2013).

16. D. Sekiba, N. Takemoto, M. Okada, S. Ishii, T. Sakurai, K. Akimoto, Hydrogen isotope tracer experiment in a-C:H film deposition: Reactive RF magnetron sputtering with CH_4 and D_2, Diamond & Related Materials **27-28**, 60-63 (2012).

17. H. Tsuchida, S. Tomita, K. Nishimura, R. Murakoshi, M. Naitoh, K. Sasa, S. Ishii, A. Yogo and A. Itoh, Properties of fast carbon cluster micro beams produced with a tapered capillary, Nucl. Instrum. Methods Phys. Res. B **293**, 6-10 (2012).

18. L. Kong, A. Uedono, S. V. Smith, Y. Yamashita, and I. Chironi, Synthesis of silica nanoparticles using oil-in-water emulsion and the porosity analysis, J. Sol.-Gel Sci. Technol. **64**, 309-314 (2012).

19. A. Uedono, T. Moriya, T. Tsutsui, S. Kimura, N. Oshima, R. Suzuki, S. Ishibashi, H. Matsui, M. Narushima, Y. Ishikawa, M. Graf, and K. Yamashita, Vacancy-type defects introduced by gas cluster ion-implantation on Si studied by monoenergetic positron beams, Jpn. J. Appl. Phys. **51**, 111801(1-5) (2012).

20. A. Uedono, S. Ishibashi, T. Watanabe, X. Q. Wang, S. T. Liu, G. Chen, L. W. Sang, M. Sumiya, and B. Shen, Vacancy-type defects in InxGa1‑xN alloys probed using a monoenergetic positron beam, J. Appl. Phys. **112**, 104507(1-5) (2012).

21. W. Zhou, Z. Chen, N. Oshima, K. Ito, B. E. O’ Rourke, R. Kuroda, R. Suzuki, H. Yanagishita, T. Tsutsui, A. Uedono, and N. Hayashizaki, In-situ characterization of free-volume holes in polymer thin films under controlled humidity conditions with an atmospheric positron probe microanalyzer, Appl. Phys. Lett. **101**, 104102(1-3) (2012).

22. A. E. Hughes, S. Mayo, Y. S. Yang, T. Markley, S. V. Smith, S. Sellaiyan, A. Uedono, S. G. Hardina, and T. H. Mustera, Using X-ray tomography, PALS and Raman spectroscopy for characterization of inhibitors in epoxy coatings, Progress in Organic Coatings **74**, 726-733 (2012).

23. A. Uedono, S. Ishibashi, K. Tenjinbayashi, T. Tsutsui, K. Nakahara, D. Takamizu, and S. F. Chichibu, Defect characterization in Mg-doped GaN studied using a monoenergetic positron beam, J. Appl. Phys. **111**, 014508(1-6) (2012).

24. A. Uedono, Y. Yamashita, T. Tsutsui, Y. Dordi, S. Li, N. Oshima, and R. Suzuki, Vacancy clustering and its dissociation process in electroless deposited copper films studied by monoenergetic positron beams, J. Appl. Phys. **111**, 104506(1-5) (2012).

25. S. F. Chichibu, K. Hazu, Y. Ishikawa, M. Tashiro, H. Namita, S. Nagao, K. Fujito, and A. Uedono, Time-resolved photoluminescence, positron annihilation, and Al0.23Ga0.77N/GaN heterostructure growth studies on low defect density polar and nonpolar freestanding GaN substrates grown by hydride vapor phase epitaxy, J. Appl. Phys. **111**, 103518(1-11) (2012).

26. A. Uedono, K. Tenjinbayashi, T. Tsutsui, Y. Shimahara, H. Miyake, K. Hiramatsu, N. Oshima, R. Suzuki, and S. Ishibashi, Native cation vacancies in Si-doped AlGaN studied by monoenergetic positron beams, J. Appl. Phys. **111**, 013512(1-5) (2012).

27. M. Sometani, R. Hasunuma, M. Ogino, H. Kuribayashi, Y. Sugahara, A. Uedono, and K. Yamabe, Variation of chemical vapor deposited SiO2 density due to generation and shrinkage of open space during thermal annealing, Jpn. J. Appl. Phys. **51**, 021101(1-3) (2012).

28. T. Kawasaki, M. Takahashi, T Ohhara, I. Tanaka, K. Kusaka, T. Hosoya, T. Yamada and K. Kurihara, Structure of Morpholinium Tribromoplumbate C4H8ONH2PbBr3 studied by the single-crystal neutron diffraction, J. Phys. Soc. Jpn., **81**, 094602-1 – 6 (2012).

29. E. Kita, H. Yanagihara, K. Mibu, T. Niizeki, J. Inoue, Development of Functional Magnetic Materials Free of Platinum Group Elements with Controlled Interfaces, Magnetics Jpn., 7, 308-313 (2012)

6.2 International conferences

1. Akira Ozawa, Nuclear mass measurements for the r-process in Rare-RI Ring, 1st Visiting NAOJ Fellow Workshop, Element Genesis and Cosmic Chemical Evolution: r-process perspective, 17-19 Oct., 2012, Wako, RIKEN Nishina Center, Japan. **(Invited talk)**

2. Akira Ozawa, Rare-RI Ring for mass measurements of exotic nuclei, A workshop on Science with Rare Ion Beams SCRIBE-2012, Variable Energy Cyclotron Centre, Sector-1, Block-AF, Bidhan Nagar (Salt Lake), Kolkata 700064, Inida, 7-9 Nov., 2012. **(Invited talk)**

3. D. Nagae, T. Niwa, Y. Ishibashi, Y. Abe, S. Fukuoka, R. Nishikiori, S. Okada, Y. Saito, N. Inaba, A. Ozawa, Y. Aoki, Development of rotating magnetic field system for the β-NMR method, The 4th Joint Meeting of the International Symposium on Hyperfine Interactions and the International Symposium on Nuclear Quadrupole Interactions (HFI/NQI 2012)

4. D. Nagae, Y. Abe, S. Okada, A. Ozawa, T. Yamaguchi, H. Suzuki, T. Moriguchi, Y. Ishibashi, S. Fukuoka, R. Nishikiori, T. Niwa, T. Suzuki, F. Suzaki, K. Sato, H. Furuki, N. Ichihashi, S. Miyazawa, Y. Yamaguchi, T. Uesaka, M. Wakasugi, Time-of-flight detector applied to mass measurements in Rare-RI Ring, 16th International Conference on Electromagnetic Isotope Separators and Techniques Related to their Applications (EMIS2012)

5. Kimikazu Sasa, The 6 MV tandem accelerator project for nuclear physics and ion beam applications at the University of Tsukuba, The 8th China-Japan Joint Nuclear Physics Symposium, 15-19 Oct., 2012, Beijing International Convention Center, Beijing, China. **(Invited talk)**

6. Kimikazu Sasa, Damage Situation of the 12UD Pelletron tandem accelerator at the University of Tsukuba by the Great East Japan Earthquake, 12th Heavy Ion Accelerator Technology Conference (HIAT2012), Chicago, Illinois USA, June 18-21, 2012.

7. K. Sasa, T. Takahashi, N. Nagashima, and K. Shima, Isotope Dependence of the Equilibrium Charge State of Cl Ions Passing through Carbon Foils, 25th International Conference on Atomic Collisions in Solids, October 21-25, 2012 Kyoto, Japan.

8. T. Komatsubara, Gamma-ray spectroscopy on 26Si -- By pass sequence for 26Al production --, New Frontiers in Nuclear Astrophysics, 18-22 June, 2012, Castiglion Fiorentino, Italy.

9. T. Komatsubara, A. Ozawa, T. Moriguchi, Y. Ito, Y. Ishibashi, Y. Abe, T. Yuasa, T. Hayakawa, T. Shizuma, K. Y. Hara, S. Kubono, H. Yamaguchi, D. Kahl, S. Hayakawa, Dam N. Binh, A. A. Chen, J. Chen, K. Setoodehnia, T. Kajino, Study of level structure on 26Si for the astrophysical interest in ^{26}Al

production, The XII International Symposium on Nuclei in the Cosmos, Proceedings of Science, XII_206, (2012), 5-10 Aug., 2012, Cairns, Australia.

10. T. Komatsubara, A. Ozawa, K. Sasa, P. Schury, D. Nagae, Y. Ito, Y. Ishibashi, Y. Abe, S. Fukuoka, R. Nishikiori, T. Niwa, H. Mita, Y. Saito, S. Okada, T. Yuasa, T. Onishi, A. Terakado, T. Hayakawa, T. Shizuma, S. Kubono, Recent research activities of nuclear astrophysics in University of Tsukuba, The XII International Symposium on Nuclei in the Cosmos, Proceedings of Science, XII_168, (2012), 5-10 Aug., 2012, Cairns, Australia.

11. T. Onishi, T. Komatsubara, T. Yuasa, T. Hayakawa, T. Shizuma, S. Kubono, The study of nucleosynthesis by means of scandium45+p reaction, Poster presentation, The XII International Symposium on Nuclei in the Cosmos, Proceedings of Science, XII_219, 5-10 Aug., 2012, Cairns, Australia.

12. T. Komatsubara, Origin of 26Al, Element Genesis and Cosmic Chemical Evolution, NAO RIKEN workshop, 17-10 Oct., 2012, RIKEN, Japan.

13. A. S. Demyanova, A. N. Danilov, S. V. Dmitriev, A. A. Ogloblin, S. A. Goncharov, N. Burtebaev, J. Burtebaeva, N. Saduev, T. L. Belyaeva, H. Suzuki, R. Nishikiori, A. Ozawa, D. Nagae, T. Moriguchi, Y. Ishibashi, H. Ooishi, K. Yokoyama, Y. Abe, K. Okumura, S. Fukuoka, S. Ito, T. Niwa, T. Komatsubara, S. Kubono, Search Neutron Halo in 9Be Excited States, Contrib.61st International Conf. "Nucleus-2011" on Problems of Nuclear Spectroscopy and Structure of Atomic Nucleus, p.66 (2011), Sarov.

14. S. Hayakawa, S. Kubono, D. Kahl, H. Yamaguchi, D. N. Binh, T. Hashimoto, Y. Wakabayashi, J. J. He, N. Iwasa, S. Kato, T. Komatsubara, Y. K. Kwon, T. Teranishi, S. Wanajo, Direct measurement of the 11C (α, p) 14N reaction at CRIB: A path from pp-chain to CNO, Proc.Carpathian Summer School of physics 2012, Exotic Nuclei and Nuclear Particle, Astrophysics IV, 24 June-7 July, 2012, L.Trache, P.G.Isar, Eds. p.339 (2012), AIP Conf.Proc.1498 (2012), Sinaia, Romania.

15. D. Sekiba, Y. Narita, S. Harada, S. Ogura, K. Fukutani, NRA for hydrogen analysis in atmospheric condition, 25th International Conference on Atomic Collisions in Solids, 21-25 October, 2012, Kyoto, Japan.

16. D. Sekiba, Y. Narita, S. Harada, M. Matsumoto, S. Ogura, H. Matsuzaki, K. Fukutani, Direct Observation of Novel Hydrogen Uptake in Nano-scale superlattice of Mg thin film by ambient NRA, 16th International Conference on Solid Films and Surfaces, 1-6 July, 2012, Genoa, Italy.

17. Y. Shiina, S. Tamura, I. Harayama, K. Yamazaki, K. Sasa, S. Ishii, and S. Tomita, Coincidence Measurement of Secondary Electrons with Scattered Ions under Irradiation of Fast Carbon-Cluster Ions, 25th International Conference on Atomic Collisions in Solids, 21-25 October, 2012, Kyoto, Japan.

18. S. Tomita, H. Tsuchida, Y. Shiina, R. Kinoshita, J. Yokoe, K. Yamazaki, S. Ishii, and K. Sasa, Transmission of Fast Carbon Cluster Ions through an Al2O3 Nano-Capillary Foil, 25th International Conference on Atomic Collisions in Solids, 21-25 October, 2012, Kyoto, Japan.

19. T. Nogami, C. Penny, L. Tai, C. Parks, P. Flaitz, A. Uedono, A. Simon, T. Bolom, C. Christiansen, A. Madan, J. Li, F. Baumann, R. Davis, T. Ryan, F. Ito, S. Choi, J. Kelly, M. He, X. Zhang, H. Kim, R. Murphy, S. Molis, J. Rowland, P. Dehaven, K. Tanwar, D. Canaperi, C-K. Hu, S. Chiang, T. Spooner, and D. Edelstein, Electromigration extendibility of Cu(Mn) alloy-seed interconnects and understanding the fundamentals, Int. Electron Devices Meeting, 10 Dec., 2012, San Francisco, CA, USA.

20. S. F Chichibu, K. Hazu, Y. Ishikawa, M. Tashiro, H. Miyake, K. Hiramatsu, and A. Uedono, Impacts of point defects on the photoluminescence lifetime of Si-doped Al0.6Ga0.4N epilayers grown on an AlN template, Int. Workshop on Nitride Semiconductors, 18 Oct., 2012, Sapporo, Japan.

21. T. Araki, N. Uematsu, M. Yutani, J. Sakaguchi, K. Wang, A. Uedono, T. Fujishima, E. Matioli, T. Palacios, and Y. Nanishi, Growth of high quality thin InN layers by RFMBE, Int. Workshop on Nitride Semiconductors, 16 Oct., 2012, Sapporo, Japan.

22. K. Furusawa, Y. Ishikawa, M. Tashiro, K. Hazu, S. Nagao, K. Fujito, A. Uedono, and S. F. Chichibu, Local carrier dynamics in freestanding GaN substrates grown by hydride vapor phase epitaxy studied using the spatio-time-resolved cathodoluminescence technique, Int. Workshop on Nitride Semiconductors, 15 Oct., 2012, Sapporo, Japan.

23. K. Patil, S. Sellaiyan, T. Lin , X. Wang , S.V. Smith, and, A. Uedono, Effect of animal protein fibre milling on free volume by positron annihilation lifetime spectroscopy, 16th Int. Conf. on Positron Annihilation, 22 Aug., 2012, Bristol, UK.

24. W. Zhou, N. Oshima, Z. Chen, K. Ito, B. E. O'Rourke, R. Kuroda R. Suzuki, H. Yanagishita, T. Tsutsui, A. Uedono, and N. Hayashizaki, Development of the humidity controlled atmospheric PPMA, 16th Int. Conf. on Positron Annihilation, 22 Aug., 2012, Bristol, UK.

25. A. Uedono, Y. Dordi, S. Li, G. Mizunaga, K. Tenjinbayashi, N. Oshima, and R. Suzuki, Agglomeration and dissociation of vacancies in electroless deposited Cu films studied by

monoenergetic positron beams, 2012 IEEE Int. Interconnect Tech. Conf., 5 June, 2012, San Jose, USA.

26. A. Sagara, M. Hiraiwa, A. Uedono, and S. Shibata, Detection and characterization of residual damage in low-dose arsenic implanted silicon after high-temperature annealing, 12th Int. Workshop on Junction Technology, 14 May, 2012, Shanghai, China.

27. M. Takahashi, W. Konishi and K. Ohshima, The electron density distribution in α-Sn, AsCA 12/CRYSTAL 28 Conference and BRAGG Symposium, 3 Dec., 2012, Adelaide.

28. Yasushi Kanke, Takuro Yoshikawa, Hideto Yanagihara, Eiji Kita, Yorihiko Tsunoda, Kiiti Siratori and Kay Kohn, Formation of stoichiometric of FeO synthesized under high pressure, 19th International Conference on Magnetism (ICM 2012), 8-13 July, 2012, Busan.

29. D. Isaka, Y. Kikuchi, A. Seki, Ka. Suzuki, M. Kishimoto, H. Yanagihara, E. Kita, Effects of viscosity of ferromagnetic dispersant on specific loss power, International Conference of the Asian Union of Magnetic Societies (ICAUMS 2012), 2pPS-119, 2-5 Oct., 2012, Nara.

30. Daichi Oka, Yasushi Hirose, Hideyuki Kamisaka, Tomoteru Fukumura, Tetsuya Hasegawa, Seiji Ito, Akira Morita, Hiroyuki Matsuzaki, Katsuyuki Fukutani, Satoshi Ishii, Kimikazu Sasa, Daiichiro Sekiba, Dielectric properties of perovskite oxynitride epitaxial thin films, APS March Meeting 2013, March 18 - 22, Baltimore, Maryland, USA.

7. THESES

Master's theses

Ryo FUNATO	Multiplicity dependence of 2-particle correlation in 200GeV p-p collisions with pythia simulation
Kaoru GUNJI	Azimuthal dependence of 2-particle interferometry in $\sqrt{s_{NN}}$=2.76TeV Pb-Pb collisions at LHC-ALICE experiment
Satoshi HORIUCHI	Reaction plane and azimuthal anisotropy measurements with participants and spectators in $\sqrt{s_{NN}}$ =2.76TeV Pb-Pb collisions at LHC-ALICE experiment
Hiroshi NAKAGOMI	Pseudo-rapidity dependence of azimuthal anisotropy with silicon vertex detector in $\sqrt{s_{NN}}$=200GeV Au-Au collisions at RHIC-PHENIX experiment
Daisuke WATANABE	Azimuthal correlation of pi0-jet in $\sqrt{s_{NN}}$=2.76TeV p-p and Pb-Pb collisions at LHC-ALICE experiment
Toshiaki YUASA	Measurement of the astrophysical S-factor for the ^{7}Li(^{3}He, p_0) ^{9}Be reaction
Takahiro NIWA	Developments of apparatus to determine the sign of nuclear magnetic moments for radioactive nuclei
Ryou NISHIKIORI	Measurements of Charge-Changing Cross Sections for Ca Isotopes and Deduction of Charge Radii
Hiroki MITA	Surface current electrostatic lens for an ion guide gas cell

Undergraduate theses

Tomo NAKAJIMA	Radon detector for radiological education - Development of teaching material and practical approach –

8. SEMINARS

2012

May 14 Rare-RI Ring Project – toward of investigation for r-process nucleosynthesis -, *Akira Ozawa (University of Tsukuba)*

Jul 18 Electron momentum distribution of organic crystals by 2D-ACAR and Leaching properties of self-healing paint for anti corrosion application, *Selvakumar Sellaiyan (University of Tsukuba)*

Aug 29 Positron Beamlines for Materials Studies and Atomic and Molecular, *James Sullivan (Australian National University)*

Nov 8 Neutron halos in excited states of stable nuclei, *Prof. A. Ogloblin (Kurchatov Institute, Moscow, Russia)*

Dec 19 Precise measurement of elliptic anisotropy with an upgraded detector and quark number scaling at $\sqrt{s_{NN}}$=200GeV Au+Au in RHIC-PHENIX, *Yosimasa Ikeda (RIKEN)*

Measurements of azimuthal correlation between jet and charged particle at LHC-ALICE experiment, *Dousatu Sakata (University of Tsukuba)*

Dec 20 Measurements of Hanbury-Brown and Twiss effect with respect to the event plane in relativistic heavy ion collisions at RHIC-PHENIX, *Takafumi Niida (University of Tsukuba)*

Measurements of Anisotropic Flow for Identified Hadrons in $\sqrt{s_{NN}}$=2.76TeV Pb + Pb Collisions at LHC-ALICE, *Masato Sano (University of Tsukuba)*

Dec 21 Mearsurments of higher-order flow harmonics and two particle, *Takahito Todoroki (University of Tsukuba)*

2013

Jan 15 Multiplicity dependence of 2-particle correlation in 200GeV p-p collisions with pythia simulation, *Ryo Funato (University of Tsukuba)*

Radon detector for radiological education - Development of teaching material and practical approach –, *Tomo Nakajima (University of Tsukuba)*

Measurements of Charge-Changing Cross Sections for Ca Isotopes and Deduction of Charge Radii, *Ryou Nishikiori (University of Tsukuba)*

Jan 16 Azimuthal correlation of pi0-jet in $\sqrt{s_{NN}}$=2.76TeV p-p and Pb-Pb collisions at LHC-ALICE experiment, *Daisuke Watanabe (University of Tsukuba)*

Surface current electrostatic lens for an ion guide gas cell, *Hiroki Mita (University of Tsukuba)*

Reaction plane and azimuthal anisotropy measurements with participants and spectators in $\sqrt{s_{NN}}$=2.76TeV Pb-Pb collisions at LHC-ALICE experiment, *Satoshi Horiuchi (University of Tsukuba)*

Jan 18 Azimuthal dependence of 2-particle interferometry in $\sqrt{s_{NN}}$=2.76TeV Pb-Pb collisions at LHC-ALICE experiment, *Kaoru Gunji (University of Tsukuba)*

Jan 18 Developments of apparatus to determine the sign of nuclear magnetic moments for radioactive nuclei, *Takahiro Niwa (University of Tsukuba)*

Pseudo-rapidity dependence of azimuthal anisotropy with silicon vertex detector in $\sqrt{s_{NN}}$ =200GeV Au-Au collisions at RHIC-PHENIX experiment, *Hiroshi Nakagomi (University of Tsukuba)*

Measurement of the astrophysical S-factor for the ^{7}Li(^{3}He, p_0) ^{9}Be reaction, *Toshiaki Yuasa (University of Tsukuba)*

Feb 28 Research program at the RCNP cyclotron facility, *Kichiji Hatanaka (Osaka University)*

9. SYMPOSIUM

=== A debrief meeting of the Pre-Strategic Initiatives ===
Inclusive liaisons around UTTAC on the recent researches and innovational uses by using accelerated ion beams and radioactive sources.

18 March 2013
Laboratory of Advanced Research B 0110

1. Openning : *E. Kita (University of Tsukuba)*

2. Status and future prospects of the 6 MV tandem accelerator project at the University of Tsukuba: *K. Sasa (University of Tsukuba)*

3. Study of nucleosynthesis by using 1MV tandetron: *T. Komatsubara (University of Tsukuba)*

4. Rare RI Ring: *D. Nagae (University of Tsukuba)*

5. High-Precision Mass Measurements at RIKEN with Multi-Reflection Time-of-Flight Mass Spectrograph: *Peter Schury (University of Tsukuba)*

6. Transport properties of chromate-containing self healing epoxy films using radiotracer, PALS and SEM: *Selvakumar Sellaiyan (University of Tsukuba)*

7. Recent studies on hydrogen in materials and renewal of hydrogen analysis systems: *D. Sekiba (University of Tsukuba)*

8. Development of ΔE-E telescope ERDA for light element analysis: *I. Harayama (University of Tsukuba)*

9. Nitrogen doping-concentration dependence in the amorphous insulator AlN for spintronics: *R. Akiyama (University of Tsukuba)*

10. Outline of irradiation facilities and their utilization sharing at JAEA Takasaki institute: *W. Yokota (JAEA)*

11. Open Advanced Research Facilities Initiative at JAEA Takasaki site: *A. Yamazaki (JAEA)*

12. Perpendicular magnetic anisotropy in $CoFe_2O_4$ epitaxial thin film: *T. Niizeki (University of Tsukuba)*

13. Evaluation of Radiation Resistance of On-board Microprocessor for University of Tsukuba Cubesat ITF-1 "YUI": *T. Kameda (University of Tsukuba)*

14. Closing remarks: *T. Komatsubara (University of Tsukuba)*

10. LIST OF PERSONNEL

Tandem Accelerator Complex

E. Kita	Director, Professor
K. Sasa	Associate Professor
T. Komatsubara	Assistant Professor
D. Sekiba	Assistant Professor
H. Kimura	Computer Engineer
H. Oshima	Electric Engineer
Y. Tajima	Mechanical Engineer
S. Ishii	Mechanical Engineer
T. Takahashi	Electric Engineer
Y. Yamato	Electric Engineer
S. Selvakumar	Research Fellow
Y. Tagishi	Research Supporter
K. Iitake	Administrative Stuff
N. Yamada	Administrative Stuff
S. Abe	Administrative Stuff

Research Members[1]

Inst. of Physics

I. Arai	T. Komatsubara	D. Nagae	A. Ozawa
K. Sasa	P. Schury		

Inst. of Applied Physics

K. Akimoto	S. Aoki	E. Kita	M. Minagawa
D. Sekiba	T. Suemasu	S. Tomita	A. Uedono
H. Yanagihara			

Inst. of Materials Science

T. Kondo	M. Takahashi

Inst. of Engineering Mechanics and Systems

K. Matsuuchi

[1]The "research members" include the authors and coauthors within 5 years back from this fiscal year, as well as the members of research projects running at UTTAC.

Inst. of Geoscience

M. Kurosawa

Inst. of Chemistry

K. Sueki

Staff of Open Advanced Facilities Initiative

H. Kudo	S. Lee	H. Naramoto	M. Matsumura
H. Muromachi			

Graduate students

Doctoral Programs of Pure and Applied Science

Y. Abe	S. Fukuoka	Y. Ishibashi	K. Ito
Y. Ito	Y. Kiguchi	K. Kurita	K. Suzuki

Master's Programs of Pure and Applied Science

K. Chito	S. Funada	N. Inaba	D. Isaka
M. Iura	I. Harayama	S. Kimura	H. Mita
A. Mori	M. Myouka	M. Mukai	R. Nishikiori
T. Niwa	S. Okada	T. Onishi	Y. Saito
Y. Shiina	N. Takemoto	T. Tsutsui	M. Uehira
Y. Yamashita	K. Yamazaki	Z. Yang	S. Yoshimatsu
T. Yuasa	Y. Watahiki	T. Watanabe	

Master's Programs of Life and Environmental Science

M. Ishikawa	Y. Sato

Undergraduates

R. Aoyama	S. Aldyyarov	F. Arai	A. Horiuchi
D. Izumi	R. Kinoshita	K. Kitajima	K. Nakashima
K.Sawahata	N. Shibayama	S. Shohata	A. Terakado
R. Watanabe	N. Yoshihara		

Scientific Gutests and Fellows

K. Awazu	National Institute of Advanced Industrial Science and Technology (AIST)
M. Fujimaki	National Institute of Advanced Industrial Science and Technology (AIST)
Y. Tosaki	National Institute of Advanced Industrial Science and Technology (AIST)
T. Hayakawa	Japan Atomic Energy Agency (JAEA)
T. Shizuma	Japan Atomic Energy Agency (JAEA)
S. Kubono	Center for Nuclear Study, Univ. of Tokyo (CNS)
A. Sato	Osaka Univ.
A. Yamamoto	High Energy Accelerator Research Organization (KEK)
T. Adachi	High Energy Accelerator Research Organization (KEK)
M. Yoshida	High Energy Accelerator Research Organization (KEK)
N. Kawamura	High Energy Accelerator Research Organization (KEK)
K. Shimomura	High Energy Accelerator Research Organization (KEK)
P. Strasser	High Energy Accelerator Research Organization (KEK)
T. Nakamoto	High Energy Accelerator Research Organization (KEK)
M. Iio	High Energy Accelerator Research Organization (KEK)
K. Yoshimura	High Energy Accelerator Research Organization (KEK)